

Froggatt-Nielsen ALP

Admir Greljo, Aleks Smolkovič, Alessandro Valenti

*Department of Physics, University of Basel,
Klingelbergstrasse 82, CH-4056 Basel, Switzerland*

E-mail: admir.greljo@unibas.ch, aleks.smolkovic@unibas.ch,
alessandro.valenti@unibas.ch

ABSTRACT: The Froggatt-Nielsen (FN) mechanism, a prominent framework for explaining the observed flavor hierarchies, generically predicts the existence of an axion-like particle (ALP). This work examines a class of FN models based on \mathbb{Z}_N discrete symmetries. We chart the allowed parameter space from a set of theoretical considerations and construct explicit renormalizable completions with minimal field content necessary to generate consistent textures. We then conduct comprehensive phenomenological analyses of two particularly elegant \mathbb{Z}_4 and \mathbb{Z}_8 models, highlighting the interplay between the effects of the ALP and the associated UV fields. We find that the FN scale can be as low as a few TeV.

Contents

1	Introduction	1
2	\mathbb{Z}_N Froggatt-Nielsen	3
3	The minimal model: \mathbb{Z}_4	7
3.1	Setup	7
3.2	Observables	12
3.3	Summary of the results	25
4	A finer model: \mathbb{Z}_8	28
5	Conclusion	32
A	UV and EFT parameters matching	33
A.1	\mathbb{Z}_4 model	33
A.1.1	EFT	33
A.1.2	UV	34
A.2	\mathbb{Z}_8 model	37
B	Derivation of the ALP couplings	37

1 Introduction

The observed pattern of fermion masses and mixings cannot be explained within the Standard Model (SM). Despite being generated from Yukawa interactions with a single Higgs field, one particularly intriguing aspect is the presence of roughly two-order-of-magnitude mass hierarchies between consecutive generations of all three types of charged fermions: up quarks, down quarks, and charged leptons. Additionally, the CKM mixing matrix [1, 2] is approximately a unit matrix, with hierarchies evident in its off-diagonal elements. In stark contrast, the neutrino sector displays a different behavior. Apart from the small overall mass scale, neutrino oscillations reveal large mixing angles and a seemingly anarchic flavor structure. The origin of generation hierarchies in the charged fermion sector, in contrast to the neutrino sector, necessitates an organizing principle beyond the SM.

The Froggatt-Nielsen (FN) mechanism [3–5] is a prototypical example of how approximate flavor symmetries can be used to generate Yukawa textures. This framework introduces a global $U(1)_{\text{FN}}$ symmetry, with different generations assigned different integer charges and a symmetry-breaking spurion $\epsilon \ll 1$ carrying a unit charge. By judiciously selecting these charges, one can construct Yukawa matrices Y_{ij}^f that exhibit a desired suppression factor $\epsilon^{n_{ij}}$. The simplicity of a FN model often conflicts with its ability to

accurately fit the observed flavor parameters [6, 7]. Opting for simpler charge assignments, with a relatively small largest integer charge, results in increased variance in the $\mathcal{O}(1)$ ultraviolet (UV) parameters. Nonetheless, such scenarios might be preferable from a simplicity perspective, given the uncertainties in the distribution of marginal couplings in the UV.

A straightforward way to realize ϵ is through the spontaneous symmetry breaking of a perturbatively exact global $U(1)_{\text{FN}}$ symmetry. This involves a complex scalar field Φ (a SM gauge singlet) with charge 1, which acquires a vacuum expectation value (VEV) $\langle \Phi \rangle = v_\Phi/\sqrt{2}$. Additionally, this framework assumes a gap between v_Φ and the common UV scale M , which underlies the generation of the FN effective field theory (EFT) operators. Consequently, $\epsilon = v_\Phi/\sqrt{2}M$.

As a result of a spontaneously broken continuous global symmetry, a Goldstone boson emerges in the spectrum, dominating infrared (IR) physics. This boson is not exactly massless due to the chiral anomaly with QCD, where non-perturbative instanton effects endow it with a mass, making it the QCD axion [8–10]. The QCD axion, proposed to address the strong CP problem, has recently been the focus of extensive theoretical [11] and experimental studies [12]. The concept of the *axiflavor* [13] or *flaxion* [14] is particularly compelling, as it simultaneously addresses two structural issues of the Standard Model: the flavor puzzle and the strong CP problem. This leads to intriguing phenomenology, characterized by the interplay between astrophysical and flavor physics constraints. Notably, the flavor constraints from $K^+ \rightarrow \pi^+ a$ impose the most stringent limits on the FN breaking scale, requiring $v_\Phi \gtrsim \mathcal{O}(10^{12})$ GeV, as detailed in [15].

The $U(1)$ symmetry can be explicitly broken in various ways, which would undermine its solution to the strong CP problem. The most problematic and perhaps unavoidable breaking arises from Planck-scale suppressed operators, leading to the axion quality problem [16–20]. The primary objective of this work is to explore a broader parameter space for the FN axion-like particle (ALP) beyond the axiflavor limit while delegating the resolution of the strong CP problem to another source. Explicit breaking can arise from operators of different dimensions. For instance, consider a soft breaking by a $m^2\phi^2$ operator, which predicts the ALP mass $m_a \sim m$. A consistency condition is required to avoid disrupting the FN EFT power counting and maintaining the desired textures: $m_a \lesssim v_\Phi$.

A systematic approach to exploring this terrain involves considering perturbatively exact discrete subgroups. In this work, we focus on \mathbb{Z}_N . We find that the simplest consistent model in non-supersymmetric theories has $N = 4$ and already fits the observed flavor parameters at the level of recently proposed $SU(2)$ gauged flavor models [21, 22] or flavor deconstruction examples [23, 24]. Increasing N allows for a finer fit to the observed fermion masses and mixings. For instance, we demonstrate that \mathbb{Z}_8 can realize the same Yukawa structure as the recently proposed $U(2)_{q+e^c+u^c} \times \mathbb{Z}_2$ symmetry [25].

Imposing a discrete symmetry instead of a continuous one eliminates the presence of a Goldstone boson in the theory. Specifically, for \mathbb{Z}_4 , no light states are expected, with $m_a \sim v_\Phi$ predicted from the Φ^4 term in the scalar potential. A light ALP is anticipated for $N > 4$, with its mass generated by a higher-dimensional operator. In fact, the same scale M responsible for the Yukawa textures can also generate the ALP mass, as illustrated later by the *wheel* models (see Fig. 2). A natural outcome of this class of models is an FN ALP

with mass \gtrsim GeV, where the decay $K^+ \rightarrow \pi^+ a$ is kinematically forbidden, as illustrated by the \mathbb{Z}_8 model in Section 4.

This raises an intriguing question: what is the lowest FN scale that remains compatible with experimental constraints? This is a quantitative question with an interesting interplay between ALP-induced effects and UV contributions. In this paper, we conduct a thorough phenomenological study performing precision calculations in explicit renormalizable models, completing the FN \mathbb{Z}_4 and \mathbb{Z}_8 structures with minimalistic ingredients. The philosophy here is that rather than estimating UV contributions through FN EFT power counting, we introduce only the necessary UV field content to realize the FN mechanism and study its irreducible effects. As we demonstrate for the chosen models, the limit on v_Φ is weaker than the one estimated using the FN EFT. In contrast to the axiflavor case, this scenario motivates direct searches for heavy new physics at future colliders.

The paper is organized as follows. In Section 2, we provide a theoretical discussion of \mathbb{Z}_N models, charting the parameter space of the FN ALP. Section 3 focuses on constructing a concrete model based on \mathbb{Z}_4 symmetry, fitting the SM flavor parameters, and presenting a comprehensive survey of experimental bounds. In Section 4, we construct and examine an explicit \mathbb{Z}_8 model. Finally, in Section 5, we conclude our study. Technical details are discussed in the Appendices.

2 \mathbb{Z}_N Froggatt-Nielsen

This section introduces a class of discrete FN models based on \mathbb{Z}_N symmetries and provides a theoretical discussion of the ALP parameter space.

Yukawa textures

Consider an EFT comprised of the SM matter content supplemented by a singlet complex scalar field Φ . Both Φ and the SM fermions are assumed to be charged under a global, perturbatively exact¹ \mathbb{Z}_N symmetry, with $[\Phi] = 1$. The mechanism generating hierarchies in the SM Yukawas is of a Froggatt-Nielsen type:

$$-\mathcal{L} \supset \sum_{f,F} \left[x_{ij}^f \left(\frac{\Phi}{M} \right)^{n_{ij}^f} + x_{ij}^{f'} \left(\frac{\Phi^*}{M} \right)^{n_{ij}^{f'}} \right] \bar{F}_{L,i} H f_{R,j} + \{\tilde{H}\} + \text{h.c.}, \quad (2.1)$$

where $x_{ij}^f, x_{ij}^{f'}$ are a priori $\mathcal{O}(1)$ couplings, and n_{ij}^f and $n_{ij}^{f'}$ are determined by the different \mathbb{Z}_N charges of the SM fields. Here, we assume a common mass scale M that generates the effective operators. The term $\{\tilde{H}\}$ is a shorthand notation for the interactions involving $\tilde{H} \equiv \varepsilon H^*$, while f and F denote SM $SU(2)_L$ singlets and doublets, respectively. H is uncharged under \mathbb{Z}_N , $[H] = 0$.

It is instructive to think of $\mathbb{Z}_N \subset U(1)$. The $U(1)$ -breaking but \mathbb{Z}_N -preserving interactions involving Φ^* (Φ) represent an important difference compared to the “standard” $U(1)$ case. The \mathbb{Z}_N , but not the $U(1)$, allows the replacement $\Phi^{n_{ij}^f} \rightarrow (\Phi^*)^{N-n_{ij}^f}$ in Eq. (2.1),

¹For realistic choices of the chiral fermion charges, the \mathbb{Z}_N symmetry is typically anomalous.

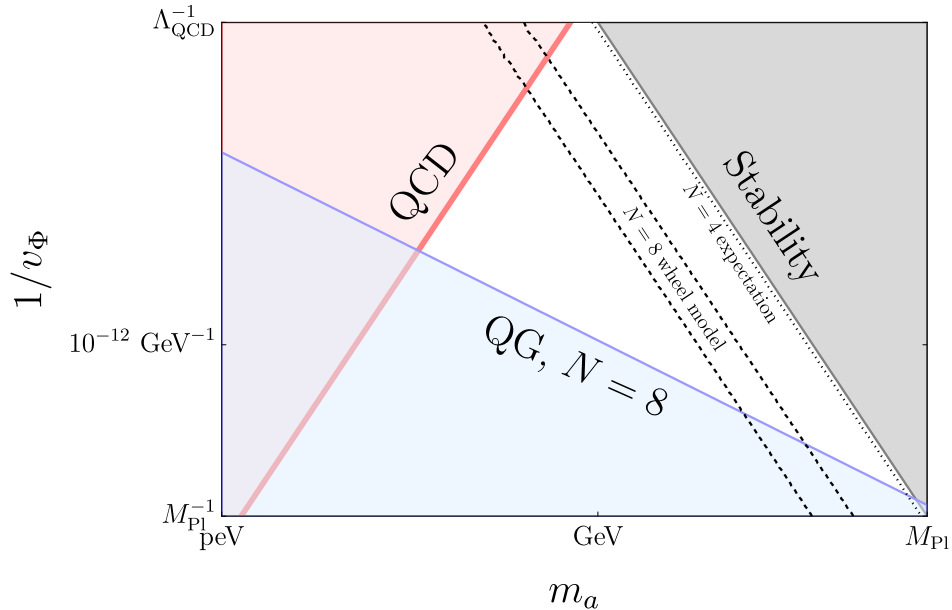


Figure 1: Theoretical constraints on the FN ALP, presented in the $(m_a, 1/v_\Phi)$ plane, arising from Eqs. (2.6), (2.10), and (2.11), with $\lambda = 0.5$. The plots have been drawn for $N = 4$ and 8; in particular, the thickness of the darker gray and red lines represents the variability of the boundary from $N = 8$ (less constraining) to $N = 4$ (more constraining). The expectation for a representative $N = 4$ model with $\lambda'_4 = \lambda/4$ is depicted with a dotted line, while the band enclosed by the dashed lines corresponds to the expectation around Eq. (2.9) for a $N = 8$ “wheel” model. For details, see Section 2.

since $[\Phi]^* = -[\Phi] \equiv (N - [\Phi]) \pmod{N}$. To avoid spoiling the hierarchies generated exclusively by $\langle \Phi \rangle$, it is required that $n_{ij}^f \leq \lfloor \frac{N}{2} \rfloor$. Therefore, special care must be taken with charge assignments to ensure the desired textures. A sufficient condition is that chiral fermions of the SM are assigned charges from the set $\{0, \dots, \lfloor \frac{N}{2} \rfloor\}$. For example, the smallest group that generates hierarchies between consecutive families by setting each family distinct charges $\{2, 1, 0\}$ is \mathbb{Z}_4 instead of \mathbb{Z}_3 .² Therefore, we will focus only on models with $N \geq 4$.

The numerical value for the spurion $\epsilon = \langle \Phi \rangle / \sqrt{2}M$ depends non-trivially on N and the specific details of the model. However, a simple estimate can be made by requiring the largest hierarchy to be saturated by $\epsilon^{\lfloor \frac{N}{2} \rfloor} \sim y_e/y_t$, where the ratio of the electron to top quark Yukawa couplings $y_e/y_t \sim 10^{-6}$. Since $\epsilon \xrightarrow{N \rightarrow \infty} 1$, large N setups are disfavored not only from the simplicity perspective but also due to concerns regarding the consistency of the FN EFT expansion.

Charting the ALP

Theoretical constraints that define the ALP’s parameter space of interest are illustrated in Fig. 1. This figure presents various constraints, which will be discussed below, in the plane

²In this work, we focus on non-supersymmetric theories. Holomorphy, however, would make the \mathbb{Z}_3 symmetry eligible. For a study of \mathbb{Z}_N FN models in supersymmetric context, see [26].

of ALP mass versus the inverse FN scale. The most general potential compatible with the \mathbb{Z}_N symmetry reads

$$V(\Phi) = -m^2|\Phi|^2 + \frac{1}{2}\lambda|\Phi|^4 - \frac{1}{4}\frac{\lambda'_N}{M_\Phi^{N-4}}[\Phi^N + (\Phi^*)^N] + \dots, \quad (2.2)$$

where without loss of generality, we take $\lambda'_N \in \mathbb{R}_{>0}$. For simplicity, we are neglecting any portals with the SM Higgs doublet and further higher-dimensional operators, which will lead to subleading corrections in the following discussion.

Let us employ a convenient parametrization $\Phi = \left(\frac{v_\Phi + \rho}{\sqrt{2}}\right) e^{ia/v_\Phi}$, where ρ and a represent the radial and angular (ALP) modes, respectively, with $\langle \Phi \rangle = v_\Phi/\sqrt{2}$. The SM Yukawa hierarchies are explained by a small parameter $\epsilon \equiv v_\Phi/(\sqrt{2}M)$ after expanding Eq. (2.1). Since, in general, M and M_Φ may differ, we define an effective coupling

$$\lambda'_{4,\text{eff}} = \lambda'_N \left(\frac{M}{M_\Phi}\right)^{N-4} \epsilon^{N-4}. \quad (2.3)$$

The minima of the potential in Eq. (2.2) are set at $v_\Phi^2 = 2m^2/(\lambda - N\lambda'_{4,\text{eff}}/4)$ and $\langle a/v_\Phi \rangle = 2\pi k/N$, $k = 1, 2, \dots, N$. The masses of the radial and angular modes read

$$m_\rho^2 = \left(\lambda - \frac{1}{8}N(N-2)\lambda'_{4,\text{eff}}\right)v_\Phi^2 \quad \text{and} \quad m_a^2 = \frac{1}{8}N^2\lambda'_{4,\text{eff}}v_\Phi^2. \quad (2.4)$$

They satisfy a sum rule:

$$m_\rho^2 + \left(\frac{N-2}{N}\right)m_a^2 = \lambda v_\Phi^2. \quad (2.5)$$

This, combined with the stability conditions $m_\rho^2 \geq 0$ and $m_a^2 \geq 0$, provides an admissible range for the ρ and a masses:³

$$\begin{aligned} 0 &\leq m_\rho^2 \leq \lambda v_\Phi^2, \\ 0 &\leq m_a^2 \leq \left(\frac{N}{N-2}\right)\lambda v_\Phi^2. \end{aligned} \quad \text{[Stability condition]} \quad (2.6)$$

The excluded region is shown in gray in Fig. 1. With marginal coupling λ of $\mathcal{O}(1)$, we generally expect $m_\rho \sim v_\Phi$. The $N = 4$ case is unique because the U(1)-breaking operator is renormalizable, resulting in $m_a \sim v_\Phi$ for $\lambda'_N \sim \mathcal{O}(1)$ and, consequently, no ALP.⁴ However, for $N > 4$, there is an ALP with mass $m_a \ll v_\Phi$.

Let us sketch a renormalizable UV model example that generates λ'_N for $N > 4$ and predicts the ALP mass. Any completion with only a minimal set of vector-like fermions

³This also holds when taking into account possible subleading corrections to Eq. (2.2) by defining effective couplings $\lambda_{\text{eff}} = \lambda(1 + \mathcal{O}(\epsilon^2))$ and $\lambda'_{4,\text{eff}} = \lambda'_N (M/M_\Phi)^{N-4} \epsilon^{N-4} (1 + \mathcal{O}(\epsilon^2))$. Higher-order harmonics cannot, however, be described in this simple picture. They are suppressed by a factor of ϵ^N compared to the leading term and can thus be safely neglected.

⁴The stability of the \mathbb{Z}_4 potential requires $\lambda'_4 < \lambda$. In the phenomenology section, we will also consider $\lambda'_N \ll 1$, in which case a is an ALP.

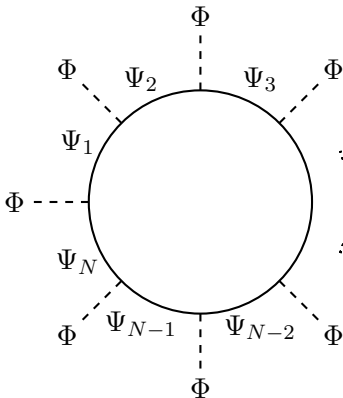


Figure 2: The “wheel” diagram generating the $U(1)_{\text{FN}}$ breaking term $\Phi^N + (\Phi^*)^N$. For details see Section 2.

(VLFs) required to generate Yukawa operators in Eq. (2.1) with desired textures typically leads to an accidental $U(1)_{\text{FN}}$ symmetry when these fields are integrated out, thus failing to generate λ'_N . An elegant mechanism to generate λ'_N would be to consider a *full* set of VLFs Ψ_k with \mathbb{Z}_N charges $[\Psi_k] = k$ and couplings $\sum_k y_k \Phi \bar{\Psi}_{L,k+1} \Psi_{R,k}$. The “wheel” diagram in Fig. 2 predicts

$$\frac{\lambda'_N}{M_\Phi^{N-4}} \sim \frac{1}{M_\Psi^{N-4}} \frac{\prod_k y_k}{16\pi^2}, \quad (2.7)$$

under the assumption of approximately degenerate Ψ_i masses.⁵

Incidentally, a subset of these VLFs, with the appropriate couplings, is sufficient to generate the Yukawa operators in Eq. (2.1). Therefore, in this class of models,

$$M \sim M_\Phi \sim M_\Psi. \quad (2.8)$$

This, finally, allows us to predict the ALP mass using Eq. (2.4),

$$\frac{m_a}{v_\Phi} \sim \frac{1}{8\pi} N \epsilon^{\frac{N}{2}-2} \sqrt{\prod_k y_k}, \quad (2.9)$$

where we take an estimate for $\epsilon \sim (y_e/y_t)^{\lfloor \frac{N}{2} \rfloor^{-1}}$, as discussed earlier. The prediction for the $N = 8$ case is shown in Fig. 1 as a region within the two black dashed lines which represent the variation $0.001 < \sqrt{\prod_k y_k} < 0.2$.⁶

This mechanism might, however, not be present at all, and the $U(1)_{\text{FN}}$ -breaking term in Eq. (2.2) could be generated by UV physics at scales M_Φ significantly larger than M .

⁵A straightforward mechanism to achieve this would be to introduce an additional real scalar field χ such that $(\chi, \Phi, \Psi_{R,k})$ are odd under a new \mathbb{Z}_2 symmetry. When χ acquires a non-zero vacuum expectation value, the interactions $\chi \bar{\Psi}_{L,k} \Psi_{R,k}$ result in comparable masses among all VLFs.

⁶Choosing y_k from a flat distribution in the $(0, 1)$ range, there is 90% probability for $\sqrt{\prod_k y_k}$ to be above (below) 0.001 (0.2).

In the most extreme scenario, the $U(1)_{\text{FN}}$ symmetry is broken solely by quantum gravity effects $M_{\Phi} \sim M_{\text{Pl}}$, which are expected to break any global symmetry [27].⁷ If this were the case, the coupling $\lambda'_{4,\text{eff}}$ would be lower bounded as $\lambda'_{4,\text{eff}} \gtrsim 16\pi^2(M/M_{\text{Pl}})^{N-4}\epsilon^{N-4}$, barring any fine-tuning on Planck-suppressed operators.⁸ This leads, in turn, to a lower bound on the ALP mass:

$$m_a^2 \gtrsim 8\pi^2 \left(\frac{N^2}{2^{N/2}} \right) \left(\frac{v_{\Phi}}{M_{\text{Pl}}} \right)^{N-4} v_{\Phi}^2. \quad [\text{QG condition}] \quad (2.10)$$

This lower bound is analogous in spirit to the constraint on the dimension of PQ-breaking operators encountered in the well-known QCD axion quality problem [16–20]. The “excluded” region for $N = 8$ is shown in blue in Fig. 1.

Finally, one should not forget QCD itself and its contribution to the axion mass, which is approximately given by $(m_a^2)_{\text{QCD}} \sim m_{\pi}^2 f_{\pi}^2 c_a^2 / v_{\Phi}^2$, where c_a is the anomaly coefficient entering $(c_a g_s^2 / 32\pi^2) G\tilde{G}$, and we approximate $c_a \sim N$. As the physical mass of the ALP is given by the sum of this contribution and the one of Eq. (2.4), any value of m_a lower than that of the single contributions requires a non-trivial cancellation. Avoiding this tuning can then be stated as

$$m_a \gtrsim (m_a)_{\text{QCD}}. \quad [\text{QCD condition}] \quad (2.11)$$

The red region shown in Fig. 1 does not satisfy this condition.⁹

To conclude, Eqs. (2.6), (2.10), and (2.11) together define an acceptable region for m_a and v_{Φ} that a \mathbb{Z}_N FN model should respect. This corresponds to the white region in Fig. 1, where we also show model expectations for $N = \{4, 8\}$ as discussed above.

3 The minimal model: \mathbb{Z}_4

This section constructs and thoroughly analyses an explicit \mathbb{Z}_4 FN model. We begin in Section 3.1 by defining a concrete renormalizable model that realizes the \mathbb{Z}_4 FN texture, and we examine the EFT structure it generates. Following this, Section 3.2 offers a comprehensive analysis of the various observables predicted by the model. Section 3.3 collects constraints in (m_a, v_{Φ}^{-1}) plane and discusses their broader implications.

3.1 Setup

The \mathbb{Z}_4 symmetry offers the simplest realization capable of generating the SM fermion hierarchies. It features a renormalizable potential given by the $N \rightarrow 4$ limit of Eq. (2.2), ensuring no massless spin-0 states exist. Therefore, this case can be considered minimal in terms of UV matter content, as it only requires completing the Yukawa operators in Eq. (2.1).

⁷In this scenario, we assume that \mathbb{Z}_N symmetry is protected, possibly through an appropriate gauging mechanism [28–31].

⁸Here M_{Pl} denotes the reduced Planck mass, $M_{\text{Pl}} \simeq 2.4 \times 10^{18}$ GeV.

⁹In the presence of multiple ALPs, this condition applies only to the linear combination entering the QCD potential. Hence, there might be additional lighter fields [32].

Fields	SU(3) _C	SU(2) _L	U(1) _Y	\mathbb{Z}_4
$q_{1,2,3}$	3	2	$\frac{1}{6}$	$\{2, 1, 0\}$
ℓ_i	1	2	$-\frac{1}{2}$	0
$e_{1,2,3}$	1	1	-1	$\{-2, -1, 0\}$
u_i	3	1	$\frac{2}{3}$	0
d_i	3	1	$-\frac{1}{3}$	0
Q_2^a	3	2	$\frac{1}{6}$	0
Q_1	3	2	$\frac{1}{6}$	1
E_2^a	1	1	-1	0
E_1	1	1	-1	1
H	1	2	$\frac{1}{2}$	0
Φ	1	1	0	1

Table 1: Field content of the UV model as described in Section 3. The rows in this table are grouped into four categories. The first and second represent left and right chiral fermions, respectively. The third consists of vector-like fermions, and the last comprises scalars. Flavor indices are denoted as $i = 1, 2, 3$ and $a = 1, 2$. See Section 3.1 for details.

UV model. The field content of a particular model incarnating this idea is listed in Table 1. Apart from Φ and the SM fields, the model includes only the addition of vector-like quarks $Q_1, Q_2^{a=1,2}$ and vector-like leptons $E_1, E_2^{a=1,2}$.¹⁰ The non-trivial FN charges under the \mathbb{Z}_4 symmetry are $[Q_1] = -[E_1] = 1$. The only charged SM fields are q and e , with $[q_1] = -[e_1] = 2$ and $[q_2] = -[e_2] = 1$.¹¹ All the other fields are taken as \mathbb{Z}_4 -neutral, except Φ . The Yukawa sector of the most general renormalizable Lagrangian compatible with this symmetry reads¹²

$$\begin{aligned}
\mathcal{L}_{\text{UV}} \supset & x_1^q \Phi \bar{q}_1 Q_1 + x_{12}^{qa} \Phi \bar{Q}_1 Q_2^a + x_2^{qa} \Phi \bar{q}_2 Q_2^a - y_j^{da} \bar{Q}_2^a H d_j - y_j^{ua} \bar{Q}_2^a \tilde{H} u_j \\
& + x_1^e \Phi \bar{E}_1 e_1 + x_{12}^{ea} \Phi \bar{E}_2^a E_1 + x_2^{ea} \Phi \bar{E}_2^a e_2 - y_i^{ea} \bar{\ell}_i H E_2^a \\
& - z_j^d \bar{q}_3 H d_j - z_j^u \bar{q}_3 \tilde{H} u_j - z_i^e \bar{\ell}_i H e_3 + \text{h.c.} .
\end{aligned} \tag{3.1}$$

¹⁰Alternatively, an even more minimal completion involves replacing VLFs with three additional Higgs doublets carrying \mathbb{Z}_4 charges of $\{1, 2, 3\}$. Their masses are $\mathcal{O}(M)$, and they do not develop a VEV.

¹¹This charge assignment is inspired by the recently proposed $U(2)_{q+e}$ flavor symmetry [25]. Charging under the flavor group only left-handed quarks and right-handed leptons produces the observed mass hierarchies of electrically charged fermions and the mixing hierarchies of left-handed quarks while maintaining an anarchic flavor structure for neutrinos, ensuring large neutrino mixing. Our \mathbb{Z}_4 is the smallest flavor symmetry resulting in similar Yukawa textures as predicted by $U(2)_{q+e}$ of [25].

¹²Note that Eq. (3.1) respects an accidental $U(1)_{\text{FN}}$. If we would have chosen a \mathbb{Z}_3 symmetry instead of \mathbb{Z}_4 , additional couplings, such as $\bar{q}_1 \Phi^* Q_2^a$, would appear, violating $U(1)_{\text{FN}}$. This would disrupt the desired Yukawa textures, as discussed below Eq. (2.1).

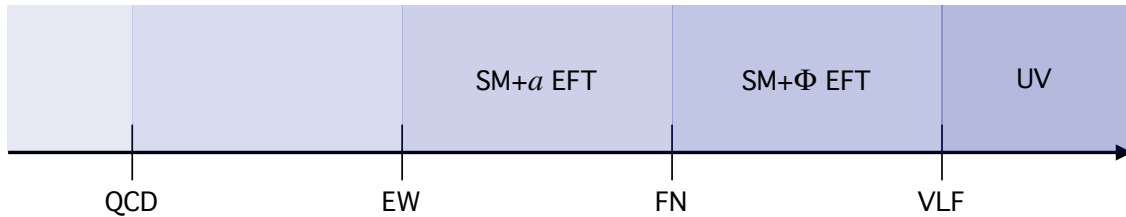


Figure 3: Illustration of the hierarchical scales within the model and the corresponding layers of effective field theory descriptions.

Flavor symmetries of the kinetic terms are used to perform field redefinitions and eliminate mass mixings between chiral and vector-like fermions of the same representation without any loss of generality. The specific basis and parameterization used are detailed in A.1.2.

Tower of EFTs. A systematic analysis of this model involves constructing a tower of effective field theories, as illustrated in Fig. 3. In the first step, the VLF states are integrated out, matching to the SM+ Φ EFT. The resulting set of local higher-dimensional operators can be categorized into two broad classes based on their involvement of the Φ field. First are operators that include the Φ field. A subset of these include Eq. (2.1), which will generate the SM Yukawa couplings at the FN scale v_Φ upon matching to the next EFT, the SM+ a EFT. This class of operators also generates a couplings. As already discussed, m_a derived in Eq. (2.4) is governed by λ'_N . Although the natural expectation $\lambda'_N \sim 1$ predicts $m_a \sim v_\Phi$, in this section, we treat λ'_N as a free parameter that can be arbitrarily small.¹³ Our goal is to explore a broader parameter space of ALP masses, deriving general lessons that relate to $N > 4$ models where ALP is expected to be light. Second, another class of operators exists that does not involve the Φ field. These operators violate the accidental flavor symmetries of the SM and induce significant UV contributions to rare and forbidden SM transitions, as we will see in a moment.

Generating the SM Yukawas. Integrating out the VLF at the tree-level leads to the effective Yukawa Lagrangian of Eq. (2.1) with $x_{ij}^{f'} = 0$ and

$$n_{ij}^d = n_{ij}^u = n_{ij}^e = \begin{pmatrix} 2 & 2 & 2 \\ 1 & 1 & 1 \\ 0 & 0 & 0 \end{pmatrix}. \quad (3.2)$$

Representative Feynman diagrams are shown in Fig. 4. The matching of x_{ij}^f to the UV parameters in Eq. (3.1) is provided in Appendix A, together with an explicit benchmark point in the parameter space correctly reproducing the SM fermion masses and mixings, see Eqs. (A.11) and (A.12). Interestingly, their values can be correctly predicted with most of the UV couplings in Eq. (3.1) within a factor of 10 from each other. This stems from the fact that the light SM Yukawas are expressed as products of many UV couplings, which

¹³It is technically natural to take $\lambda'_4 \ll 1$, though this opposes the spirit of our narrative.

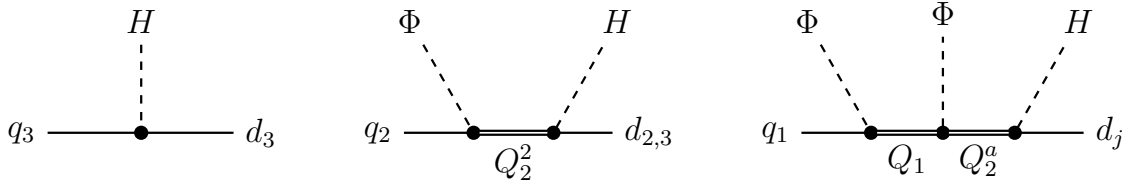


Figure 4: Leading diagrams in the \mathbb{Z}_4 model generating effective down-quark Yukawa operators in Eq. (2.1), and analogously for up quarks and charged leptons. For further details, refer to Section 3.1.

can naturally contribute to the hierarchy if these are somewhat small, say $\mathcal{O}(0.3)$.¹⁴ The only exceptions are y_b and y_τ , which are here not dynamically generated, and hence we require them to be of $\mathcal{O}(10^{-2})$.

ALP couplings. For the upcoming flavor phenomenology discussion, we express the couplings of the radial and angular modes of Φ in the SM fermion mass basis as

$$\mathcal{L} \supset - \sum_{f=u,d,e} c_{ij}^f \bar{f}_{Li} (\rho + ia) f_{Rj} + \text{h.c.} + \text{h.o.}, \quad (3.3)$$

where the coupling matrices can be generally expressed as

$$c^f = \frac{1}{v_\Phi} \left[\left(U_L^{f\dagger} Q^f U_L^f \right) \hat{m}^f - \hat{m}^f \left(U_R^{f\dagger} Q^f U_R^f \right) \right]. \quad (3.4)$$

Here U_L and U_R are the left- and right-handed fermion rotation matrices that diagonalize the corresponding mass terms, \hat{m} are the diagonal fermion mass matrices, and Q are diagonal matrices encoding the SM fermion FN charges. The derivation of this formula is presented in Appendix B. In our concrete realization of the FN model, only the left-handed quarks are charged, and the down-type quark coupling matrix can be written as

$$c^d = \frac{1}{v_\Phi} \left(V_{\text{CKM}}^\dagger Q^d V_{\text{CKM}} \right) \hat{m}^d, \quad (3.5)$$

where we assumed that the CKM matrix is fully given by $U_L^d = V_{\text{CKM}}$. This is a sensible assumption as the bigger hierarchies in the up sector lead to much more suppressed mixing angles in U_L^u , as shown in App. A. Interestingly, the down-quark flavor-changing neutral currents due to a, ρ are then fully determined by the measured values of the down-quark masses and the CKM matrix, up to the overall normalization of v_Φ . Using the Wolfenstein parameterization, we get

$$c^d = \frac{1}{v_\Phi} \begin{pmatrix} 2m_d & \lambda m_s & A\lambda^3 m_b (-2i\eta + 2\rho - 1) \\ \lambda m_d & m_s & A\lambda^2 m_b \\ A\lambda^3 m_d (2i\eta + 2\rho - 1) & A\lambda^2 m_s & A^2 \lambda^4 m_b \end{pmatrix}, \quad (3.6)$$

¹⁴A similar effect is observed in Fig. 3 of [22].

where in each entry, we keep only the leading nontrivial term in λ . The c_{33}^d entry is small as a result of the fact that both the left and right components of the third generation are uncharged under \mathbb{Z}_4 . Hence, the coupling only arises due to a small mixing. This is a peculiarity of the \mathbb{Z}_4 symmetry, which does not hold for larger N where one attempts to address the smallness of y_b and y_τ dynamically. For the purposes of phenomenology, we also report the lowest order in which we get complex off-diagonal entries:

$$\begin{aligned}
v_\Phi c_{12}^d &= \lambda m_s - \lambda^3 m_s/2 + \lambda^5 m_s (A^2(i\eta - \rho + 1) - 1/8), \\
v_\Phi c_{21}^d &= \lambda m_d - \lambda^3 m_d/2 + \lambda^5 m_d (A^2(-i\eta - \rho + 1) - 1/8), \\
v_\Phi c_{23}^d &= A\lambda^2 m_b + A\lambda^4 m_b (-2i\eta + 2\rho - 1/2), \\
v_\Phi c_{32}^d &= A\lambda^2 m_s + A\lambda^4 m_s (2i\eta + 2\rho - 1/2).
\end{aligned} \tag{3.7}$$

Similarly, for c^u and c^e we find

$$\begin{aligned}
c^u &= \frac{1}{v_\Phi} \begin{pmatrix} 2m_u & m_c \frac{m_u}{m_c} \frac{z_{u2}}{z_{u1}} & m_t \frac{m_u}{m_t} \frac{2y_{u2}z_{u3} - y_{u3}z_{u2}}{y_{u2}z_{u1}} \\ m_u \frac{m_u}{m_c} \frac{z_{u2}}{z_{u1}} & m_c & m_t \frac{m_c}{m_t} \frac{y_{u3}}{y_{u2}} \\ m_u \frac{m_u}{m_t} \frac{2y_{u2}z_{u3}^* - y_{u3}z_{u2}}{y_{u2}z_{u1}} & m_c \frac{m_c}{m_t} \frac{y_{u3}}{y_{u2}} & m_c \frac{m_c}{m_t} \frac{y_{u3}^2}{y_{u2}^2} \end{pmatrix}, \\
c^e &= \frac{1}{v_\Phi} \begin{pmatrix} 2m_e & m_e \frac{m_e}{m_\mu} \frac{z_{e2}}{z_{e1}} & m_e \frac{m_e}{m_\tau} \frac{2y_{e2}z_{e3}^* - y_{e3}z_{e2}}{y_{e2}z_{e1}} \\ m_\mu \frac{m_e}{m_\mu} \frac{z_{e2}}{z_{e1}} & m_\mu & m_\mu \frac{m_\mu}{m_\tau} \frac{y_{e3}}{y_{e2}} \\ m_\tau \frac{m_e}{m_\tau} \frac{2y_{e2}z_{e3} - y_{e3}z_{e2}}{y_{e2}z_{e1}} & m_\tau \frac{m_\mu}{m_\tau} \frac{y_{e3}}{y_{e2}} & m_\mu \frac{m_\mu}{m_\tau} \frac{y_{e3}^2}{y_{e2}^2} \end{pmatrix},
\end{aligned} \tag{3.8}$$

where $y_{u_i}, z_{u_i}, y_{e_i}, z_{e_i}$ are parameters that are not determined within the EFT but can be correlated to the UV parameters in Eq. (3.1) as shown in App. A. The matrices have been written factorizing the mixing, which renders evident the fact that ALP-induced flavor violation is suppressed by the ratio of the fermion masses. Again, the couplings to the third generation are small due to the fact that these are not charged under \mathbb{Z}_4 . We stress that c^d of Eq. (3.6) features the same pattern upon recognizing that $\lambda \sim m_d/m_s$, $A\lambda^2 \sim m_s/m_b$ and $A\lambda^3 \sim m_d/m_b$.

\mathbb{Z}_4 -symmetric UV operators. Integrating out VLFs at the UV matching scale directly generates certain SMEFT operators that violate approximate flavor symmetries and are crucial for the phenomenological discussion. We refer to these as ‘‘VLF contributions’’, and we will carefully study their interplay with the ALP contributions. Already at the tree level, the model generates

$$(H^\dagger i \overleftrightarrow{D}_\mu H)(\bar{\ell}_i \gamma^\mu \ell_j), \quad (H^\dagger i \overleftrightarrow{D}_\mu H)(\bar{d}_i \gamma^\mu d_j), \quad (H^\dagger i \overleftrightarrow{D}_\mu H)(\bar{u}_i \gamma^\mu u_j), \tag{3.9}$$

with arbitrary flavor structure and Wilson coefficients $\sim M^{-2}$. These operators provide a leading contribution to $\Delta F = 1$ transitions such as e'/ϵ , $\mu \rightarrow e$ conversion, $K_L \rightarrow \mu^+ \mu^-$, etc. Additionally, under renormalization, they mix into $\Delta F = 2$ operators. The primary $\Delta F = 2$ contributions, however, arise from four-fermion operators generated through one-

loop matching at the UV scale. These are

$$(\bar{d}_i \gamma^\mu d_j)(\bar{d}_k \gamma_\mu d_l), \quad (\bar{u}_i \gamma^\mu u_j)(\bar{u}_k \gamma_\mu u_l), \quad (3.10)$$

with Wilson coefficients $\sim (4\pi M)^{-2}$. The flavor violation in Eq. (3.10) is expected to be of $\mathcal{O}(1)$ since our model does not impose any selection rules. This will result in stringent constraints from neutral meson mixing, most notably ϵ_K . Finally, lepton flavor violating four-fermion operators

$$(\bar{\ell}_i \gamma^\mu \ell_j)(\bar{d}_k \gamma_\mu d_l), \quad (\bar{\ell}_i \gamma^\mu \ell_j)(\bar{u}_k \gamma_\mu u_l), \quad (3.11)$$

are generated at the one-loop level and they represent the leading contribution to LFV meson decays, such as $K_L \rightarrow e\mu$.

In the following subsection, we will review all the relevant observables and provide precise details to support these statements.

3.2 Observables

The \mathbb{Z}_4 model provides a concrete framework to explore the interplay between the VLF and the ALP contributions. As discussed above, we treat the $U(1)_{\text{FN}}$ -breaking parameter λ'_N as a free parameter and consider a broad range of ALP masses, temporarily setting aside the expectation of $m_a \sim v_\Phi$ for $\lambda'_N \sim 1$. By allowing $\lambda'_N \ll 1$, we can explore the ALP phenomenology in a concrete model. As we will argue later, the results should remain qualitatively consistent across the entire class of FN ALP models. Our presentation in this subsection is organized by observables, highlighting contributions from each source.¹⁵

Rare meson decays

ALP. In the $U(1)_{\text{FN}}$ limit, a becomes very light, making the “invisible” meson decay $K \rightarrow \pi a$ the most significant constraint on v_Φ , followed by $B \rightarrow K^{(*)} a$. The decay rate is given by

$$\Gamma(M_1 \rightarrow M_2 a) = \frac{m_{M_1}^3}{64\pi} \lambda^{1/2} \left(\frac{m_{M_2}}{m_{M_1}}, \frac{m_a}{m_{M_1}} \right) \left(\frac{1 - m_{M_2}^2/m_{M_1}^2}{m_{q_i} - m_{q_j}} \right)^2 |f_{M_1 \rightarrow M_2}(m_a^2)|^2 \times \left[|c_{ij}^f|^2 + |c_{ji}^f|^2 - 2 \text{Re} c_{ij}^f c_{ji}^f \right], \quad (3.12)$$

where $\lambda(x, y) = (1 - (x + y)^2)(1 - (x - y)^2)$ and q_i, q_j refer to quarks from the parton-level transition. The quantity $f_{M_1 \rightarrow M_2}(m_a^2)$ is the form factor parameterizing the hadronic matrix element evaluated at $q^2 = m_a^2$, where $\langle M_2(p_2) | \bar{q}_i q_j | M_1(p_1) \rangle = f_{M_1 \rightarrow M_2}(q^2)(m_{M_1}^2 - m_{M_2}^2)/(m_{q_i} - m_{q_j})$ with $q = p_1 - p_2$. For these, we rely on their determinations as reported in Refs. [42–48]. The constraints we consider include the combined E787 and E949 analysis $\text{Br}(K^+ \rightarrow \pi^+ E_{\text{miss}}) < 9.5 \times 10^{-11}$ [49], the BaBar bound $\text{Br}(B \rightarrow K^* E_{\text{miss}}) < 1.0 \times 10^{-4}$ [50] and the recent Belle II measurement $\text{Br}(B^+ \rightarrow K^+ \bar{\nu}\nu) = (2.3 \pm 0.7) \times 10^{-5}$ [51]. For the latter, given the current $\approx 2.4\sigma$ tension between the SM prediction and the experimental

¹⁵For related phenomenological ALP studies see [15, 33–41].

value, we employ the 3σ bound on $\text{Br}(B \rightarrow Ka)$ derived in [52] (see also [53]). For $m_a < m_{K,B}$, these observables provide the most significant bounds on the FN scale, with $v_\Phi \gtrsim 10^{11}$ GeV for kaon decay and $v_\Phi \gtrsim 10^7$ GeV for B decay.

Importantly, these bounds apply only if the ALP behaves as an invisible final state. This requires that the distance traveled by the ALP after production and before an eventual decay exceeds the length of the detector, $l_a > l_{\text{detector}}$, where

$$l_a = \frac{c|p_a|}{m_a \Gamma_a}. \quad (3.13)$$

In this expression, $|p_a|$ represents the axion momentum in the laboratory frame, and Γ_a is its total decay width. We approximate $l_{\text{detector}} \approx 1$ m and assume the decaying meson is at rest.¹⁶

If the ALP can decay inside the detector, the signatures differ. Prominent constraints in our model involve leptonic and semi-leptonic decays of flavored mesons [54]. The rate for lepton-flavor-violating decays is straightforward and reads

$$\begin{aligned} \Gamma(M \rightarrow \ell_i \bar{\ell}_j) = & \frac{f_M^2 m_M}{64\pi} \frac{\lambda^{1/2} \left(\frac{m_{\ell_i}}{m_M}, \frac{m_{\ell_j}}{m_M} \right)}{(m_{q_k} + m_{q_l})^2} \frac{[|c_{kl}^q|^2 + |c_{lk}^q| + 2 \text{Re } c_{kl}^q c_{lk}^q]}{(1 - m_a^2/m_M^2)^2 + m_a^2 \Gamma_a^2/m_M^4} \\ & \times \left[(|c_{ij}^e|^2 + |c_{ji}^e|^2) \left(1 - \frac{m_{\ell_i}^2 + m_{\ell_j}^2}{m_M^2} \right) + 4 \text{Re } c_{ij}^e c_{ji}^e \frac{m_{\ell_i} m_{\ell_j}}{m_M^2} \right], \end{aligned} \quad (3.14)$$

where $q = u, d$. Subscripts q_k and q_l refer to the underlying quark transition, Γ_a is the total width of a and $\langle 0 | \bar{q}_k \gamma^5 q_l | M \rangle = f_M m_M^2 / (m_{q_k} + m_{q_l})$. We take the 95% CL bounds on the branching ratios from Table 2 of [55]. As expected, the strongest constraint comes from $\text{Br}(K_L \rightarrow e\mu) < 6.3 \times 10^{-12}$ [56], which plateaus for $m_a \lesssim m_{K_L}$, setting $v_\Phi \gtrsim 10$ TeV. Bounds from other scalar meson decays are at least two orders of magnitude less stringent, while vector meson decays are negligible due to their large width. For completeness, our numerical analysis includes constraints from unflavored meson decays. The expressions differ slightly due to the anomaly contribution [54]. However, the large width of these mesons leads to much weaker bounds.

Lepton flavor conserving decays also play an important role, as the diagonal couplings in Eq. (3.8) are larger than the off-diagonal ones, which are further suppressed by the small hierarchical mixing. The expression for the total decay rate is complicated by the interference between the SM and ALP contributions. To handle this properly, we compute the corresponding bounds using `flavio` [57], leveraging the fact that in these processes, the virtual momentum of the ALP is essentially fixed by the meson mass. Our findings show that the strongest constraint arises from $K_L \rightarrow \mu\mu$, which plateaus at roughly $v_\Phi \gtrsim 70$ TeV.

Semileptonic decays are enhanced in the on-shell ALP production regime $m_{M_1} - m_{M_2} >$

¹⁶These considerations also apply to $M_1 \rightarrow M_2 \rho$ decays for a very light ρ , with the replacements $m_a \rightarrow m_\rho$ and $c_{ij}^f \rightarrow -ic_{ij}^f$. This applies to all processes discussed in this section; hence, we will report explicit expressions involving only a , particularly since a light ρ is less motivated.

$m_a > m_{\ell_i} + m_{\ell_j}$, in which the branching ratio can be factorized as

$$\text{Br}(M_1 \rightarrow M_2^{(*)} \ell_i \bar{\ell}_j) \simeq \text{Br}(M_1 \rightarrow M_2^{(*)} a) \text{Br}(a \rightarrow \ell_i \bar{\ell}_j), \quad (3.15)$$

where

$$\begin{aligned} \Gamma(a \rightarrow f_i \bar{f}_j) &= m_a \frac{N_c}{16\pi} \lambda^{1/2} \left(\frac{m_i}{m_a}, \frac{m_j}{m_a} \right) \\ &\times \left[\left(|c_{ij}^f|^2 + |c_{ji}^f|^2 \right) \left(1 - \frac{m_i^2 + m_j^2}{m_a^2} \right) + 4 \text{Re} c_{ij}^f c_{ji}^f \frac{m_i m_j}{m_a^2} \right]. \end{aligned} \quad (3.16)$$

Defining $\langle M_2^*(p_2) | \bar{q}_k \gamma^5 q_l | M_1(p_1) \rangle = -2i f^*(q^2)_{M_1 \rightarrow M_2^*} (\epsilon \cdot q) m_{M_2^*} / (m_{q_k} + m_{q_l})$ with $q = p_1 - p_2$ and $\epsilon_\mu = \epsilon_\mu(p_2)$ the polarization vector of M_2^* , one finds

$$\begin{aligned} \Gamma(M_1 \rightarrow M_2^* a) &= \frac{m_{M_1}^3}{64\pi} \lambda^{3/2} \left(\frac{m_{M_2^*}}{m_{M_1}}, \frac{m_a}{m_{M_1}} \right) \frac{|f_{M_1 \rightarrow M_2^*}^*(m_a^2)|^2}{(m_{q_k} + m_{q_l})^2} \\ &\times \left[|c_{kl}^f|^2 + |c_{lk}^f|^2 + 2 \text{Re} c_{kl}^f c_{lk}^f \right]. \end{aligned} \quad (3.17)$$

In this category, we can identify two classes of experimental searches. Searches for prompt decays reconstruct the 3-body vertex with a typical resolution of approximately $\mathcal{O}(100) \mu\text{m}$. When applying constraints from such searches, we require $l_a \lesssim 100 \mu\text{m}$, unless stated otherwise. Searches for displaced vertices, instead, provide bounds based on the lifetime of the long-lived particle. We will distinguish between these two types of searches and their corresponding bounds in the following discussion.

Let us first consider *prompt* decays. For lepton flavor-violating ones, we revisit the processes studied in Ref. [55]. The strongest constraint comes from $\text{Br}(B \rightarrow K \mu \tau) < 7.7 \times 10^{-6}$ [58], followed by $\text{Br}(B \rightarrow \pi \mu \tau) < 5.9 \times 10^{-5}$ [59], and $\text{Br}(B \rightarrow K^* \mu \tau) < 9.8 \times 10^{-6}$ [60]. For lepton flavor conserving decays, the situation is complicated by current tensions between SM predictions and experimental values of various branching ratios and angular observables involving the underlying $b \rightarrow s \mu \mu$ transition [61–65]. In contrast, the theoretically cleaner $R_{K^{(*)}}$ ratios are measured to be consistent with SM expectations [66, 67]. Here, we only consider these ratios to derive constraints on the ALP contributions, roughly setting $v_\Phi \gtrsim \text{TeV}$.

For *displaced* vertex signatures, we consider the bounds from LHCb on $B \rightarrow K^{(*)} \mu \mu$ [68, 69], which sets exclusion limits in the region $10^3 \text{ GeV} \lesssim v_\Phi \lesssim 10^7 \text{ GeV}$, see also Ref. [70]. Additionally, we consider the decays $B \rightarrow K \gamma \gamma$ and $K \rightarrow \pi \gamma \gamma$, computed analogously using the well-known expressions for $\text{Br}(a \rightarrow \gamma \gamma)$ found in [71]. We employ the bound on $\text{Br}(K \rightarrow \pi \gamma \gamma)$ for long-lived ALPs from NA64 [72] and the bound on $\text{Br}(B \rightarrow K \gamma \gamma)$ from BaBar [73]. These constraints are similar, setting $v_\Phi \gtrsim \text{TeV}$, with the former being slightly stronger but applicable over a much narrower interval of ALP masses.

VLF. Let us now turn to the UV contributions obtained by integrating out VLFs to generate local operators that directly affect rare meson decays. As mentioned earlier, the leading effects come from operators not involving the Φ field. In particular, the Higgs-current

operators

$$\begin{aligned}\mathcal{O}_{Hd}^{ij} &= (H^\dagger i\overleftrightarrow{D}_\mu H)(\bar{d}_R^i \gamma^\mu d_R^j), \\ \mathcal{O}_{Hu}^{ij} &= (H^\dagger i\overleftrightarrow{D}_\mu H)(\bar{u}_R^i \gamma^\mu u_R^j),\end{aligned}\tag{3.18}$$

are generated already at the tree level integrating out the heavy Q_2^a . The corresponding Wilson coefficients read

$$C_{Hd}^{ij} = \frac{y_j^{da} y_i^{da*}}{2M_{Q_2}^2}, \quad C_{Hu}^{ij} = \frac{y_j^{ua} y_i^{ua*}}{2M_{Q_2}^2}.\tag{3.19}$$

These operators induce flavor-changing Z -boson couplings to right-handed quarks after electroweak symmetry breaking [74]. Focusing on down quark transitions, we define the weak effective Hamiltonian for $d_j \rightarrow d_i \ell \ell$ and $d_j \rightarrow d_i \nu \nu$ as $\mathcal{H}_{\text{eff}} = -\mathcal{N} \sum_i C_i O_i + \text{h.c.}$, where $\mathcal{N} = \frac{4G_F}{\sqrt{2}} \frac{e^2}{16\pi^2} V_{tj} V_{ti}^*$ and the sum runs over the semileptonic local operators. Then, the \mathcal{O}_{Hd} operator is matched by a Z exchange to

$$C_{10}^{ij\ell\ell} = \frac{1}{2\mathcal{N}} C_{Hd}^{ij}, \quad C_R^{ij\nu\nu} = \frac{1}{\mathcal{N}} C_{Hd}^{ij},\tag{3.20}$$

with $O_{10}^{ij\ell\ell} = (\bar{d}_i \gamma_\mu P_R d_j)(\bar{\ell} \gamma^\mu \gamma_5 \ell)$ ¹⁷ and $O_R^{ij\nu\nu} = (\bar{d}_i \gamma_\mu P_R d_j)(\bar{\nu} \gamma_\mu (1 - \gamma_5) \nu)$. We stress that these contributions are lepton flavor universal. We use `flavio` [57] to obtain the bounds from meson decays with charged or neutral leptons in the final states. The leading constraints are due to kaon decays, in particular to $K \rightarrow \pi \nu \nu$ setting the leading constraint $v_\Phi \gtrsim 200$ GeV. Purely leptonic kaon decays $K_L \rightarrow ee, \mu\mu$ offer a slightly worse sensitivity, $v_\Phi \gtrsim 100$ GeV. B and D decays lead to subleading constraints.

Lepton flavor-violating contributions can arise in two ways. The first is via the exchange of a Z boson, with one insertion of Eq. (3.18) and one of

$$\begin{aligned}\mathcal{O}_{H\ell}^{(1)ij} &= (H^\dagger i\overleftrightarrow{D}_\mu H)(\bar{\ell}_R^i \gamma^\mu \ell_R^j) \\ \mathcal{O}_{H\ell}^{(3)ij} &= (H^\dagger i\overleftrightarrow{D}_\mu H)(\bar{\ell}_R^i \tau^I \gamma^\mu \ell_R^j),\end{aligned}\tag{3.21}$$

generated at tree level via the heavy E_2^a . The corresponding Wilson coefficients are

$$C_{H\ell}^{(1)ij} = C_{H\ell}^{(3)ij} = -\frac{y_i^{ea} y_j^{ea*}}{4M_E^2}.\tag{3.22}$$

The second way involves integrating out the VLFs at 1-loop, directly generating the 4-fermion SMEFT operator

$$\mathcal{O}_{\ell d}^{ijkl} = (\bar{\ell}_i \gamma^\mu \ell_j)(\bar{d}_k \gamma_\mu d_l),\tag{3.23}$$

¹⁷The related operator involving a vector leptonic current O'_9 is suppressed due to the small SM Z couplings to these leptonic currents.

with Wilson coefficient¹⁸

$$C_{ld}^{ijkl} = \frac{1}{128\pi^2} \left[2y_i^{ea} (y_j^{ea})^* (y_k^{da})^* y_l^{da} \frac{\log M_{E_2}^2 / M_{Q_2}^2}{M_{E_2}^2 - M_{Q_2}^2} - \frac{3}{M_{E_2}^2} y_i^{ea} (y_j^{ea})^* (z_k^d)^* z_l^d - \frac{3}{M_{Q_2}^2} z_i^{ea} (z_j^{ea})^* (y_k^{da})^* y_l^{da} \right]. \quad (3.24)$$

Despite the 1-loop factor, this provides the dominant constraint since $M_{Q_2, E_2} \gtrsim 4\pi v$. In principle, there is a third way via SMEFT (renormalization group) RG effects on Eq. (3.21). However, the RG effect is always subleading, as flavor mixing would be CKM-suppressed and thus less significant compared to the anarchic nature of the coefficient in Eq. (3.24). To establish the bounds, we map the contribution of these Wilson coefficients to the same set of lepton flavor violating decays analyzed in the ALP-mediated case, following [55]. The resulting constraints are significantly weaker compared to the lepton flavor-conserving ones obtained earlier, with the strongest being associated with $K_L \rightarrow e\mu$, leading to $v_\Phi \gtrsim 10 \text{ GeV}$.

Neutral meson mixing

One of the leading constraints for both flavorful ALP and VLQs is due to their contributions to the CP-even and CP-odd observables measured in $P^0 - \bar{P}^0$ oscillations, with $P = K, B, B_s, D$. We use `flavio` to obtain constraints on both the ALP and the VLQ contributions to the following observables: ϵ_K , measuring CP violation in kaon mixing [42, 56, 76–79],¹⁹ Δm_s (Δm_d) and $S_{\psi\phi}$ ($S_{\psi K}$) measuring the neutral meson mass difference and mixing induced CP violation in B_s (B_d) mixing [61, 80–82], and $x_{12}^{\text{Im}, D}$ measuring CP violation in D mixing [82, 83].

ALP. We write the $\Delta F = 2$ Hamiltonian in the quark mass basis as

$$\mathcal{H}_{\text{NP}}^{\Delta F=2} = C_1^{ij} (\bar{q}_L^i \gamma^\mu q_L^j)^2 + \tilde{C}_1^{ij} (\bar{q}_R^i \gamma^\mu q_R^j)^2 + C_2^{ij} (\bar{q}_R^i q_L^j)^2 + \tilde{C}_2^{ij} (\bar{q}_L^i q_R^j)^2 + C_4^{ij} (\bar{q}_R^i q_L^j) (\bar{q}_L^i q_R^j) + C_5^{ij} (\bar{q}_L^i \gamma^\mu q_L^j) (\bar{q}_R^i \gamma_\mu q_R^j) + \text{h.c.}, \quad (3.25)$$

with $q = u, d$ and i, j are flavor indices, whereas the color indices are contracted inside parentheses. Integrating out the scalar and pseudoscalar components of Φ generates $\Delta F =$

¹⁸We used Matchete [75] to obtain this and the other 1-loop Wilson coefficients presented in the paper, cross-checking the expressions with known results in the literature.

¹⁹Note that we do not use Δm_K as a constraint due to the large uncertainties in its SM prediction from long-distance contributions. Instead, we use its experimental value as an input when predicting ϵ_K . Nevertheless, we checked that saturating the experimental value of Δm_K with the NP contributions leads at most to bounds comparable to that from ϵ_K .

2 operators already at the tree level as follows

$$\begin{aligned}
C_2^{q,ij} &= -\frac{(c_{ji}^{q*})^2}{2} \left(\frac{1}{m_\rho^2} - \frac{1}{m_a^2} \right), \\
\tilde{C}_2^{q,ij} &= -\frac{(c_{ij}^q)^2}{2} \left(\frac{1}{m_\rho^2} - \frac{1}{m_a^2} \right), \\
C_4^{q,ij} &= -c_{ij}^q c_{ji}^{q*} \left(\frac{1}{m_\rho^2} + \frac{1}{m_a^2} \right).
\end{aligned} \tag{3.26}$$

Here we have assumed the ALP to be heavier than the appropriate scale of each $P - \bar{P}$ process. In the case of a light ALP, this is no longer applicable, and ALP propagator effects should be included [35]. However, in this work, we do not consider the meson mixing constraints in the case of a light ALP, as we find that parameter space is predominantly constrained by other processes, such as rare meson decays. Outside of that region, we anticipate that meson mixing observables are responsible for the strongest bound coming from ALP physics. This roughly sets $v_\Phi \gtrsim 10 \text{ TeV} \times (10 \text{ GeV}/m_a)$.

VLQ. Among the VLQs with the interaction Lagrangian defined in Eq. (3.1), Q_2^q can generate $\Delta F = 2$ operators via two effects. The first effect is obtained by integrating out Q_2^q at the tree level, as discussed in the rare meson decay case; see Eq. (3.19). The generated operators could, in principle, generate $\Delta F = 2$ operators via two insertions of the modified Z couplings. Such contributions are highly suppressed. Important effects can, however, be generated by 1-loop SMEFT RG. Performing one insertion of (3.19) and closing the loop with two Higgses and a fermion, we obtain y_t -enhanced effects by generating the left-right 4-fermion \mathcal{O}_{qd} operator (in the notation of [84]). These effects have been found to be phenomenologically relevant in Ref. [85], and we take them into account in our analysis.

The second way to generate $\Delta F = 2$ effects is from one-loop matching contributions. This directly generates 4-fermion operators required to induce such effects:

$$\begin{aligned}
\mathcal{O}_{dd}^{ijkl} &= (\bar{d}_i \gamma^\mu d_j)(\bar{d}_k \gamma_\mu d_l), \\
\mathcal{O}_{uu}^{ijkl} &= (\bar{u}_i \gamma^\mu u_j)(\bar{u}_k \gamma_\mu u_l).
\end{aligned} \tag{3.27}$$

The Wilson coefficients associated with these operators read

$$\begin{aligned}
C_{dd}^{ijkl} &= \frac{1}{64\pi^2} \frac{1}{M_{Q_2}^2} (y_i^{da})^* y_j^{da} \left[-(y_k^{db})^* y_l^{db} + 3(z_s^d)^* z_t^d \right], \\
C_{uu}^{ijkl} &= \frac{1}{64\pi^2} \frac{1}{M_{Q_2}^2} (y_i^{ua})^* y_j^{ua} \left[-(y_k^{ub})^* y_l^{ub} + 3(z_s^u)^* z_t^u \right].
\end{aligned} \tag{3.28}$$

The $\Delta F = 2$ operators are obtained by selecting $i = k$ and $j = l$. In the minimal basis defined in App. A, the terms involving z couplings do not contribute.

Employing the benchmark discussed in App. A, we find that these one-loop matching contributions offer the dominant constraint, which comes from ϵ_K , setting $v_\Phi \gtrsim 2.8 \text{ TeV}$. The rest of the $\Delta F = 2$ constraints, namely the CP-even and CP-odd observables in B_d , B_s and D -mixing, show various degrees of interplay between tree-level and one-loop

contributions of VLQs, but offer only subleading constraints of $v_\Phi \gtrsim 100$ GeV.

It is worth mentioning that also the operators $\mathcal{O}_{qd}, \mathcal{O}_{qu}$ can be generated at the one-loop level and could, in principle, lead to important effects. Indeed, the components diagonal in q do not need an insertion of Φ and hence can be generated already at dimension 6. After electroweak symmetry breaking, the rotation to the mass basis induces additional flavor violation in the down-strange sector, suppressed only by the CKM. This suppression could, in principle, be overcome by an enhancement in the observables due to the different chirality structures of the operators in such a way that the bounds become potentially important. Accidentally, in \mathbb{Z}_4 models the operator $(\bar{q}_2 \gamma^\mu q_2)(\bar{d}_i \gamma_\mu d_j)$ is generated at 1-loop with coefficient $\sim (y_i^{da} x_2^{qa})^* (y_j^{da} x_2^{qa})$ (and similarly for up-quarks), which vanishes whenever the first generator is involved (see App. A). Hence, this effect could only appear in B_s -mixing, which is not very constraining.

ϵ'/ϵ

The ϵ'/ϵ observable acts as a probe of direct CP violation in $K_L \rightarrow \pi\pi$. The current best estimate of the SM predictions is $(\epsilon'/\epsilon)_{\text{SM}} = (13.9 \pm 5.2) \times 10^{-4}$ [86–90], while the experimental world average is $(\epsilon'/\epsilon)_{\text{exp}} = (16.6 \pm 2.3) \times 10^{-4}$ [56]. We use the master formula presented in Refs. [89, 91] to compute the BSM contributions to ϵ'/ϵ as

$$\left(\frac{\epsilon'}{\epsilon}\right)_{\text{BSM}} = \sum_b P_b(\mu_{\text{ew}}) \text{Im} [C_b(\mu_{\text{ew}}) - C'_b(\mu_{\text{ew}})] , \quad (3.29)$$

where P_b parameterizes the matrix elements of the relevant four quark operators, which we consider in the JMS basis [74]. We use the numerical values reported in Table 3 of Ref. [89].

ALP. The ALP contributes to ϵ'/ϵ at the tree-level through scalar four-fermion $\Delta F = 1$ operators. In the notation of Ref. [89] these are $[O_{dd}^{S1,RR}]_{2111}, [O_{ud}^{S1,RR}]_{1121}$, and their $L \leftrightarrow R$ counterparts. However, its contributions are suppressed by first-generation quark masses. At most, this renders only subleading constraint up to $v_\Phi \gtrsim 100$ GeV.

VLF. VLQs induce flavor-violating Z -boson couplings to right-handed quarks via Eq. (3.19). As can be seen from Table 3 of Ref. [89], the largest matrix elements are due to left-right vector operators. In our setup, $[O_{dd}^{V1,LR}]_{2111}, [O_{du}^{V1,LR}]_{2111}$ are generated by integrating out the Z boson, with VLQ-induced flavor violating right-handed down quark vector currents, contracted with either left-handed up or down quark currents due to the SM Z couplings. We obtain the bound $v_\Phi \gtrsim 0.7$ TeV.

$\ell_i \rightarrow \ell_j \gamma$

Both the ALP and the VLFs generate lepton flavor-violating couplings that are strongly constrained by purely leptonic observables. Dipole transitions can be encoded in the WET Lagrangian via

$$\mathcal{L}_D \supset C_{e\gamma}^{ij} (\bar{e}_i \sigma^{\mu\nu} P_L e_j) F^{\mu\nu} + \text{h.c.} . \quad (3.30)$$

Assuming $m_{\ell_j} > m_{\ell_i}$, the branching ratio of $\ell_j \rightarrow \ell_i \gamma$ then reads [92]

$$\text{Br}(\ell_j \rightarrow \ell_i \gamma) = \frac{m_{\ell_i}^3}{4\pi\Gamma_{\ell_j}} (|C_{e\gamma}^{ij}|^2 + |C_{e\gamma}^{ji}|^2). \quad (3.31)$$

ALP. The ALP a generates these observables at the one loop. In the regime in which the ALP is much more massive than ℓ_j , the Wilson coefficient associated with the operator (3.30) reads

$$C_{e\gamma}^{ij} = \frac{e}{32\pi^2 m_a^2} \sum_{k=1,2,3} \left[\frac{1}{6} (m_{\ell_j} c_{ki}^{e*} c_{kj}^e + m_{\ell_i} c_{ik}^e c_{jk}^{e*}) - m_{\ell_k} c_{ki}^{e*} c_{jk}^{e*} \left(\frac{3}{2} + \log \frac{m_{\ell_j}^2}{m_a^2} \right) \right] \quad (3.32)$$

whereas the contribution of ρ can be obtained by the replacement $m_a^2 \rightarrow m_\rho^2$, $c \rightarrow -ic$. The contribution from Barr-Zee diagrams is relevant only for ALP masses below the charm mass, given the smallness of our ALP couplings with the top and bottom quarks. The expression for these contributions can be found in [35], and we take them into account in our final plot. The relevant current experimental bounds are $\text{Br}(\mu \rightarrow e\gamma) < 4.2 \times 10^{-13}$ [93, 94] and $\text{Br}(\tau \rightarrow \mu\gamma) < 4.4 \times 10^{-8}$ [95, 96]. Both lead to comparable bounds due to the hierarchical structure of c_{ij}^e up to $v_\Phi \gtrsim \text{TeV}$.

VLF. The operator (3.30) can also be generated by integrating out the heavy VLFs at 1-loop. The corresponding \mathbb{Z}_4 -invariant SM+ Φ terms are

$$C_{eB\Phi}^{ij} \Phi^{n_{ij}^e} \bar{\ell}_i \sigma^{\mu\nu} H e_j B_{\mu\nu} + C_{eW\Phi}^{ij} \Phi^{n_{ij}^e} \bar{\ell}_i \sigma^{\mu\nu} \tau^a H e_j W_{\mu\nu}^a, \quad (3.33)$$

where by simple dimensional analysis $C_{eB\Phi, eW\Phi}^{ij} \sim g^{(\prime)} y_*^{3+n_{ij}^e} / 16\pi^2 M^{2+n_{ij}^e}$, with y_* some representative UV coupling. After Φ condensation, this leads to the SMEFT operators $\mathcal{O}_{eB, eW}$, which combine to Eq. (3.30). Using Matchete [75], we were able to exactly extract the Wilson coefficients relevant for $\mu \rightarrow e\gamma$ and $\tau \rightarrow \mu\gamma$:

$$C_{eB\Phi}^{i2} = \frac{g'}{32\pi^2 M_{E_2}^2} \left[-\frac{1}{M_{E_1}} (x_{12}^{ea})^* x_2^{ea} x_{12}^{eb} y_i^{eb} + \frac{1}{12 M_{E_2}} \left(x_2^{ea} (x_2^{ea})^* x_2^{eb} y_i^{eb} + 2x_2^{ea} y_k^{ea} (y_k^{eb})^* y_i^{eb} \right) \right], \quad (3.34)$$

$$C_{eW\Phi}^{i2} = \frac{g}{384\pi^2 M_{E_2}^3} x_2^{ea} y_k^{ea} (y_k^{eb})^* y_i^{eb}.$$

The coefficients $C_{eB\Phi, eW\Phi}^{i3}$ are null because e_3 does not couple to any VLF, while $C_{eB\Phi, eW\Phi}^{i1}$ arise at dimension 8 since they involve a further power of Φ . Hence, $C_{eB\Phi, eW\Phi}^{i2}$ provide the leading contributions to the aforementioned transitions. Note that the couplings in Eq. (3.34) are not perfectly aligned with the effective Y_e (see App. A). This leads to a further mixing between the components of the dipoles after the diagonalization of the Yukawa with a e_i rotation. We match these coefficient to $C_{e\gamma}$ after Φ condensation via $C_{e\gamma}^{ij} = v(c_w C_{eB} - s_w C_{eW}) / \sqrt{2}$. The coefficient qualitatively scales as $C_{e\gamma}^{i2} \sim ev y_*^4 \epsilon^3 / 16\pi^2 v_\Phi^2$, that can lead to bounds on v_Φ of $\mathcal{O}(\text{TeV})$ for $y_* \sim \mathcal{O}(1)$ due to the stringent constraint on

$\mu \rightarrow e\gamma$. Precisely, employing the benchmark in App. A, we find $v_\Phi \gtrsim 150$ GeV.

$\mu \rightarrow e$ conversion in nuclei

$\mu \rightarrow e$ conversion in nuclei is one of the most constraining observables on new physics models predicting lepton flavor violation. Following Ref. [97], the operators relevant to our discussion comprise the following set

$$\begin{aligned}
O_{qq}^{VLL} &= (\bar{e}\gamma_\mu P_L \mu)(\bar{q}\gamma^\mu P_L q), \\
O_{qq}^{VLR} &= (\bar{e}\gamma_\mu P_L \mu)(\bar{q}\gamma^\mu P_R q), \\
O_{qq}^{SLL} &= (\bar{e}P_L \mu)(\bar{q}P_L q), \\
O_{qq}^{SLR} &= (\bar{e}P_L \mu)(\bar{q}P_R q), \\
O_{gg}^L &= \alpha_s m_\mu G_F (\bar{e}P_L \mu) G_{\mu\nu}^\alpha G^{\alpha\mu\nu},
\end{aligned} \tag{3.35}$$

together with their $L \leftrightarrow R$ equivalents and the dipole operators of Eq. (3.30).²⁰ The conversion rate on a nucleus N is [97–100]

$$\Gamma_{\mu \rightarrow e}^N = \frac{m_\mu^5}{4} \left| C_L^D D_N + 2 \left(G_F m_\mu m_p \tilde{C}_{(p)}^{SL} S_N^{(p)} + \tilde{C}_{(p)}^{VR} V_N^{(p)} + p \rightarrow n \right) \right|^2 + L \leftrightarrow R, \tag{3.36}$$

where $C_L^D \equiv C_{e\gamma}^{e\mu}/m_\mu$ and

$$\begin{aligned}
\tilde{C}_{p/n}^{VR} &= \sum_{q=u,d} (C_{qq}^{VRL} + C_{qq}^{VRR}) f_{Vp/n}^{(q)}, \\
\tilde{C}_{(p/n)}^{SL} &= \sum_{q=u,d,s} \frac{(C_{qq}^{SLL} + C_{qq}^{SLR})}{m_\mu m_q G_F} f_{Sp/n}^{(q)} + \tilde{C}_{gg}^L f_{Gp/n}, \\
\tilde{C}_{gg}^L &= C_{gg}^L - \frac{1}{12\pi} \sum_{q=c,b} \frac{(C_{qq}^{SLL} + C_{qq}^{SLR})}{m_\mu m_q G_F},
\end{aligned} \tag{3.37}$$

and similarly for $L \leftrightarrow R$. The vector operator nucleon form factors are $f_{Vp}^{(u)} = 2$, $f_{Vn}^{(u)} = 1$, $f_{Vp}^{(d)} = 1$, $f_{Vn}^{(d)} = 2$, while for the scalar and the gluonic form factors, we take the values as reported in Ref. [97], see also Refs. [101–104]. The most sensitive current measurement is on Au for which we have the overlap integrals $V_{\text{Au}}^{(p)} = 0.0974$, $V_{\text{Au}}^{(n)} = 0.146$, $S_{\text{Au}}^{(p)} = 0.0614$, $S_{\text{Au}}^{(n)} = 0.0918$, $D_{\text{Au}} = 0.189$ [98]. Finally, the prediction should be compared to the 90% CL limit on $\mu \rightarrow e$ conversion in gold by SINDRUM II [105]

$$\text{Br}(\mu \rightarrow e) = \frac{\Gamma(\mu^- \text{Au} \rightarrow e^- \text{Au})}{\Gamma_{\text{capt}}(\mu^- \text{Au})} < 7 \times 10^{-13}, \tag{3.38}$$

where the estimate for the capture rate can be found in [98, 106].

ALP. The ALP contributes to $\mu \rightarrow e$ conversion in multiple ways: directly generating the scalar four fermion operators O_{qq}^S at the tree level, contributing through the dipole

²⁰As for $\ell_i \rightarrow \ell_j \gamma$ processes, the contributions from Barr-Zee diagrams are relevant only for $m_a \lesssim m_c$. We take this into account in our final plot, taking the expression for these contributions from [35].

operator as in Eq. (3.32), or generating O_{gg} after integrating out the heavy SM quarks. The tree-level matching results in

$$\begin{aligned}
C_{qq}^{SLL} &= c_{qq}^{q*} c_{21}^{e*} \left(\frac{1}{m_\rho^2} - \frac{1}{m_a^2} \right), \\
C_{qq}^{SLR} &= c_{qq}^q c_{21}^{e*} \left(\frac{1}{m_\rho^2} + \frac{1}{m_a^2} \right), \\
C_{qq}^{SRL} &= c_{qq}^{q*} c_{12}^e \left(\frac{1}{m_\rho^2} + \frac{1}{m_a^2} \right), \\
C_{qq}^{SRR} &= c_{qq}^q c_{12}^e \left(\frac{1}{m_\rho^2} - \frac{1}{m_a^2} \right),
\end{aligned} \tag{3.39}$$

Note that for coherent conversion in Eq. (3.36) only the scalar quark current operator enters, thus the pseudoscalar a contributions above cancel as c_{qq}^q are real. We obtain bounds of up to $v_\Phi \gtrsim \text{TeV}$.

VLF. Muon conversion into an electron in the field of a nucleus can also proceed through SM Z exchange, with flavor-violating couplings to leptons induced by the operator in Eq. (3.21) and exploiting the SM coupling to quarks. The vector operators in Eq. (3.35) are generated with [107]

$$\begin{aligned}
C_{qq}^{VLL} &= \Gamma_{e\mu}^{\ell L} \frac{1}{M_Z^2} \Gamma_{qq}^L, \\
C_{qq}^{VLR} &= \Gamma_{e\mu}^{\ell L} \frac{1}{M_Z^2} \Gamma_{qq}^R.
\end{aligned} \tag{3.40}$$

The Z boson couples to quarks via $\Gamma_{qq}^{L,R}$ in the standard way, whereas the $Z\mu e$ coupling reads

$$\Gamma_{e\mu}^{\ell L} = \frac{g_2}{2c_W} v^2 \left(C_{H\ell}^{(1)12} + C_{H\ell}^{(3)12} \right). \tag{3.41}$$

Using our benchmark, we obtain the bound $v_\Phi \gtrsim 1.1 \text{ TeV}$.

Rare lepton decays

Rare lepton decays comprise a wide set of observables, including flavor-violating $\ell_i \rightarrow \ell_j + \text{invisible}$, $\ell_i \rightarrow \ell_j \ell_k \ell_k$ and $\ell_i \rightarrow M^{(*)} \ell_j$. As usual, we will focus on ALP and VLF contributions separately.

ALP. As with mesons, we begin by discussing flavor-violating decays with an invisible ALP as a final state. Bounds on the decay of a muon into an electron and an invisible scalar have been set at TRIUMF [108] and from TWIST [109], while analogous bounds for τ decays have been reported by Belle II [110]. The relevant formula for such decays is

$$\Gamma(f_i \rightarrow f_j a) = m_i \frac{N_c}{32\pi} \lambda^{1/2} \left(\frac{m_a}{m_i}, \frac{m_j}{m_i} \right) \left[\left(|c_{ij}^f|^2 + |c_{ji}^f|^2 \right) \left(1 - \frac{m_a^2 - m_j^2}{m_i^2} \right) - 4 \text{Re} c_{ij}^f c_{ji}^f \frac{m_j}{m_i} \right], \tag{3.42}$$

and we again impose $\ell_a \gtrsim 1$ m for the ALP to be considered invisible. The bounds on v_Φ that we obtain are almost always superseded by the one coming from $K \rightarrow \pi a$.

Next we consider the $\ell_i \rightarrow M^{(*)} \ell_j$ processes, where M is a scalar (vector) meson. In the ALP-mediated case, the decay rate for decays in flavored scalar mesons closely resembles one of the leptonic flavored meson decays (3.14):

$$\Gamma(\ell_i \rightarrow M \ell_j) = \frac{f_M^2 m_{\ell_i}}{128\pi} \frac{\lambda^{1/2} \left(\frac{m_M}{m_{\ell_i}}, \frac{m_{\ell_j}}{m_{\ell_i}} \right)}{(m_{q_k} + m_{q_l})^2} \frac{[|c_{kl}^q|^2 + |c_{lk}^q| + 2 \operatorname{Re} c_{kl}^q c_{lk}^q]}{(1 - m_a^2/m_M^2)^2 + m_a^2 \Gamma_a^2/m_M^4} \quad (3.43)$$

$$\times \left[(|c_{ij}^e|^2 + |c_{ji}^e|^2) \left(1 - \frac{m_M^2 - m_{\ell_j}^2}{m_{\ell_i}^2} \right) - 4 \operatorname{Re} c_{ij}^e c_{ji}^e \frac{m_{\ell_j}}{m_{\ell_i}} \right].$$

The expression for decays to vector mesons vanishes at tree level because of the scalar nature of the interaction mediated by a , while for unflavored mesons, the situation is once again complicated by the overlap with $G\tilde{G}$ [54]. Since the experimental constraints on the branching ratio of these decays are all quite similar, the most constraining ones are those involving decays of taus into muons [56] and all lead to comparable bounds $v_\Phi \gtrsim \text{TeV}$.

For $\ell_i \rightarrow \ell_j \ell_k \bar{\ell}_k$, the branching ratio in the presence of an ALP is enhanced in the on-shell production regime $2m_k < m_a < m_i - m_j$. Here, the ratio can be factorized as

$$\operatorname{Br}(\ell_i \rightarrow \ell_j \bar{\ell}_k \ell_k) \simeq \operatorname{Br}(\ell_i \rightarrow \ell_j a) \operatorname{Br}(a \rightarrow \bar{\ell}_k \ell_k). \quad (3.44)$$

with relevant decay rates given in Eqs. (3.16) and (3.42). The situation for these decays is similar to that of semileptonic meson decays in that we can distinguish prompt and displaced vertex searches. Among the former, we find that the strongest constraint is due to $\operatorname{Br}(\tau \rightarrow 3\mu) < 2.5 \times 10^{-8}$ at 95% CL [111] constraining up to $v_\Phi \gtrsim 10^5$ GeV. Decays into electrons are suppressed due to the hierarchical nature of c^e ; even the strong bounds from $\mu \rightarrow 3e$ [112] do not beat $\tau \rightarrow 3\mu$. Searches for displaced vertices are instead lacking in this context, although new searches have been proposed over the last years [113, 114]. To our knowledge, the only available bounds are on $\mu \rightarrow 3e$ [115] and $\mu \rightarrow e\gamma\gamma$ [116–118]. These, however, lead to completely negligible bounds in our model of the order $v_\Phi \gtrsim \text{GeV}$.

VLF. The VLLs can induce the $\ell_i \rightarrow M^{(*)} \ell_j$ decays in multiple ways: either by a double insertion of the tree-level operators in Eqs. (3.18), (3.21), a single insertion of the 1-loop generated operator in Eq. (3.23), or, for unflavored M , by a single LFV modification of the Z boson couplings from Eq. (3.21). We find that the latter effect is phenomenologically the most important. Using `flavio` [57] we obtain constraints from $\tau \rightarrow \rho \ell$ and $\tau \rightarrow \phi \ell$ [119], which are however of order $v_\Phi \gtrsim 20$ GeV and hence subleading.

Also the $\ell \rightarrow 3\ell$ decays can proceed through a Z exchange²¹ with the tree-level LFV coupling from Eq. (3.21) and an SM Z coupling. As the couplings in the VLL benchmark are anarchic, $\mu \rightarrow 3e$ is now the only phenomenologically important channel. The branching

²¹It is worth mentioning that in our model the operator $\mathcal{O}_{\ell\ell}^{ijkl} = (\bar{\ell}_i \gamma^\mu \ell_j)(\bar{\ell}_k \gamma^\mu \ell_l)$ is also generated at 1-loop integrating out the VLLs. This effect is, however, subleading compared to the tree-level one.

ratio prediction reads [107]

$$\text{Br}(\mu \rightarrow 3e) = \frac{m_\mu^5}{1536\pi^3 m_Z^4 \Gamma_\mu} \left(2|\Gamma_{e\mu}^{\ell L} \Gamma_{ee}^{\ell L}|^2 + |\Gamma_{e\mu}^{\ell L} \Gamma_{ee}^{\ell R}|^2 \right), \quad (3.45)$$

with $\Gamma_{e\mu}^{\ell L}$ defined in Eq. (3.41) and with the SM Z couplings to electrons. We obtain the bound $v_\Phi \gtrsim 400$ GeV.

EDMs

Electric dipole moments are among the most sensitive probes of CP violating new physics. The strongest constraints are the ones on the electron EDM, $|d_e|/e < 5.4 \times 10^{-30}$ cm at 95% CL [120], and on the neutron EDM, $|d_n|/e < 2.6 \times 10^{-26}$ cm at 95% CL [121]. In particular, the electron EDM at leading order is directly associated with the dipole operator $\mathcal{O}_{e\gamma}$ introduced earlier [122]

$$d_e \simeq -2 \text{Im} C_{e\gamma}^{11}, \quad (3.46)$$

while the expression for the neutron EDM, in the notation of [122], reads²²

$$\begin{aligned} d_n \simeq & -0.2 d_u + 0.8 d_d - 0.003 d_s + 0.05 \hat{d}_u + 0.1 \hat{d}_d - 51 e \cdot \text{MeV} C_{G\tilde{G}} \\ & - 0.6 e \times \text{GeV} \text{Im} \left[C_{ud}^{S1,RR} + C_{ud}^{S8,RR} - C_{duud}^{S1,RR} - C_{duud}^{S8,RR} \right]^{1111}. \end{aligned} \quad (3.47)$$

In principle, our model also predicts contributions to the magnetic dipole moments, which are much less constraining than those from the EDMs.

ALP. In the heavy ALP case ($m_a \gtrsim$ GeV), the leading contribution to the eEDM can be directly read off from Eq. (3.32). The imaginary part of $C_{e\gamma}^{11}$ vanishes, meaning that no contribution to the eEDM is generated at this order. To check that NLO corrections do not lead to significant bounds, we can estimate the hypothetical constraint if an $\mathcal{O}(1)$ imaginary part in $C_{e\gamma}$ was there, obtaining the weak bound $v_\Phi > \mathcal{O}(10)$ GeV \times (GeV/ m_a), indicating that this observable is under control. For the neutron EDM, the situation is similar: the dipoles ($d_u, d_d, d_s, \hat{d}_u, \hat{d}_d$) feature an expression close to that of $C_{e\gamma}$ and are hence real. The 4-fermion operator coefficient $C_{ud}^{S1,RR}$ entering Eq. (3.47) is generated at the tree level, but features no imaginary part. An analysis analogous to the one for the eEDM reveals that the bound for a hypothetical $\mathcal{O}(1)$ phase reads $v_\Phi > \mathcal{O}(10^2)$ GeV \times (GeV/ m_a), once again negligible compared to the flavor bounds analyzed earlier. In the very light ALP case ($m_a \lesssim$ GeV), contributions to the nEDM approximate to a constant close to the previous estimate when $m_a \sim m_u$ [123]. While this could potentially lead to a bound comparable to the ones from other observables analyzed earlier, in reality, we know that this contribution is still not there due to the absence of an imaginary part in the relevant Wilson coefficients. Therefore, whatever effect may arise at NLO must be phenomenologically irrelevant. The operator $C_{G\tilde{G}}$ can be generated only at very high loop orders.

²²We omit the contribution from C_{Hud} , since in any case below the EW scale this operator can be mapped to 4-fermion operators obtained integrating out W^\pm bosons.

VLF. The VLFs generate the operators Eq. (3.33) directly contributing to the eEDM. We can estimate the size of the bound employing Eq. (3.34), that after e_i rotation generates a non-zero entry $C_{e\gamma}^{11} \sim evy_*^5\epsilon^4/16\pi^2v_\Phi^2$ with an $\mathcal{O}(1)$ imaginary part. This is a single contribution to the eEDM, which, in principle, should be added to that of the dimension-8 $C_{eB\Phi,eW\Phi}^{i,1}$, whose induced $C_{e\gamma}^{11}$ features the same scaling. However, barring accidental cancellations, this should be enough to estimate the constraint coming from the eEDM. We find the bound $v_\Phi \gtrsim 230$ GeV for our benchmark. This is interesting but again subleading compared to ϵ_K and other bounds derived earlier. For the nEDM, the bound from the dipole operators can be obtained in an analogous way to that of the eEDM. As the experimental bound on the former is 4 orders of magnitude weaker than the one on the latter, and given the same functional dependence on the UV scales and couplings (but in the quark sector), this does not lead to a competitive bound on v_Φ . The 4-fermion operators entering Eq. (3.47) are associated to \mathcal{O}_{quqd} in the SMEFT, but in the SM+ Φ EFT are uplifted to $\mathcal{O}_{quqd\Phi}^{ijkl} \sim \Phi^{n_{ik}^q}(\bar{q}_i u_j)\epsilon(\bar{q}_k d_l)$. Due to the large ϵ suppression, this does not lead to relevant constraints. Finally, the full expression for Eq. (3.47) should include also the contribution from $C_{Hud}^{ij} = -(y_i^{ua})^* y_j^{da}/M_{Q_2}^2$ [122]. We find $\text{Im} C_{Hud}^{11} = 0$; hence this cannot contribute to leading order. A hypothetical $\mathcal{O}(1)$ imaginary part would, in any case, result in the subleading $v_\Phi > |y_*| \times \mathcal{O}(10^2)$ GeV, hence NLO effects on this operator can be safely neglected. The Weinberg operator is generated only at a very high loop order.

In conclusion, the current constraints on EDMs generate only subleading bounds compared to the other observables we analyzed.

Cosmology, astrophysics, and haloscopes

We mention the impact of haloscope searches, astrophysics, and cosmology bounds on our model for completeness. Haloscope searches constrain v_Φ through the axion-photon coupling. We take the bounds from [124], rescaling the plot to adapt it to our model correctly. The usual astrophysics bounds (from [124]) are completely superseded by the bound due to $K \rightarrow \pi a$ and hence are irrelevant. For cosmology, the left part of the blue region in Fig. 5 is taken again from [124] and is dominated by the X -rays bound, assuming that the ALP constitutes a significant portion of the dark matter observed in our universe. The rightmost part is obtained via the requirement that the total ALP decay rate satisfies $\Gamma_{a,\text{tot}} \geq 3H(T_{\text{BBN}})$, where $T_{\text{BBN}} = 4$ MeV, in order to comply with the constraints from Big Bang Nucleosynthesis [125]. The rate $\Gamma_{a,\text{tot}}$ has been computed taking into account all the decay channels of the ALP in our model. For ALP masses around the QCD confinement scale, this has been approximated with a linear interpolation between $m_a \sim 3m_\pi$ and $m_a \simeq 2$ GeV, given the complications due to flavor and CP violating ALP interactions with hadrons present in our model. The impact of the heavy ρ and the VLFs is irrelevant as they quickly decay to SM particles via Eqs. (3.1) and (3.3).

Direct searches

Low-scale FN models present an exciting opportunity for direct searches at high-energy colliders. Collider searches for heavy neutral scalars and ALPs have recently received significant attention [126–133]. Light ALPs ($m_a \lesssim 10$ GeV) either escape the detector or

lead to displaced vertices. Mono- γ and mono-jet searches for light ALPs [126] are, however, not competitive with meson decays. Moving on to EW scale masses, phenomenology in this model is driven by couplings to second-generation fermions, see Eqs. (3.6) and (3.8). This is because, in the \mathbb{Z}_4 case, the bottom and tau Yukawas size are not dynamically explained (unlike in the \mathbb{Z}_8 model of Section 4). Resonant axion production at hadron colliders has been discussed in Ref. [134]. We expect the dominant channels in our case to be $gc \rightarrow ta$ and $\bar{c}c \rightarrow a$. The cross sections, computed in Fig. 11 of Ref. [134] for $v_\Phi = 0.5$ TeV, show that one should expect a large number of events. However, as discussed in [134], due to large backgrounds a dedicated detailed experimental analysis is required.

The flavor-violating ALP-top-charm coupling leads to the $t \rightarrow ca$ decay. A study of this anomalous decay has been carried out in [134], considering the current and the potential future bounds on $\text{Br}(t \rightarrow Hc)$ with $H \rightarrow \bar{b}b$ and assuming $\text{Br}(a \rightarrow \bar{b}b) > 80\%$. A major difference between ours and their scenario is the branching ratio of the decay $a \rightarrow \bar{b}b$. This would reduce the impact of this search since we expect $a \rightarrow c\bar{c}$ decay channel to dominate. A proper assessment would require repeating the numerical study from [134] within our model, which is beyond the scope of our paper. Therefore, we will not include these bounds in our figures. Even considering the nominal value they find, the bound from $\Delta F = 2$ processes remains dominant in that region. However, with future measurements, the situation might change. For light ALPs, the displaced signatures from top decays could lead to important bounds in the future [128].

For completeness, searches for vectorlike quarks and leptons at LHC set lower bounds on their masses of $\mathcal{O}(\text{TeV})$ [135, 136], which cannot compete against bounds from flavor physics in our scenario, forcing $M \approx v_\Phi/\epsilon \gtrsim \text{PeV}$.

To sum up, while the current direct searches provide subleading constraints, the situation will improve with proposed future high-energy colliders.

3.3 Summary of the results

This subsection summarizes and illustrates the main phenomenological results derived in the previous subsection. In Fig. 5, we show the exclusion contours in the $(m_a, 1/v_\Phi)$ plane for a broad range of ALP masses, $m_a \in [10^{-18}, 10^9]$ GeV. The stability region in gray, the dotted line for the $N = 4$ expectation, and the dashed line for the QCD expectation are the same as already discussed in Fig. 1. Importantly, we can immediately notice that following the $N = 4$ expectation line, the main constraint on the \mathbb{Z}_4 model is due to the vector-like fermions, illustrating the significance of a UV completion. The contour in red depicts the combined constraint due to the presence of these states in the UV, which is dominated by the CP violating kaon mixing observable ϵ_K as discussed in the previous subsection, setting $v_\Phi \gtrsim 2.8$ TeV. The answer to the question posed in the introduction, “How low can the FN symmetry-breaking scale be?”, aligns with the current energy frontier.

The ALP flavor phenomenology is less important in this particular scenario, even though it plays a major role in a large part of the parameter space as depicted by the orange contour, which combines all of the flavorful ALP constraints from the previous subsection. Notably, it sets the leading constraint on the flaxion/axiflavor scenario [13, 14] through the kinematically allowed $K \rightarrow \pi a$ decays. As already mentioned, the astrophysics

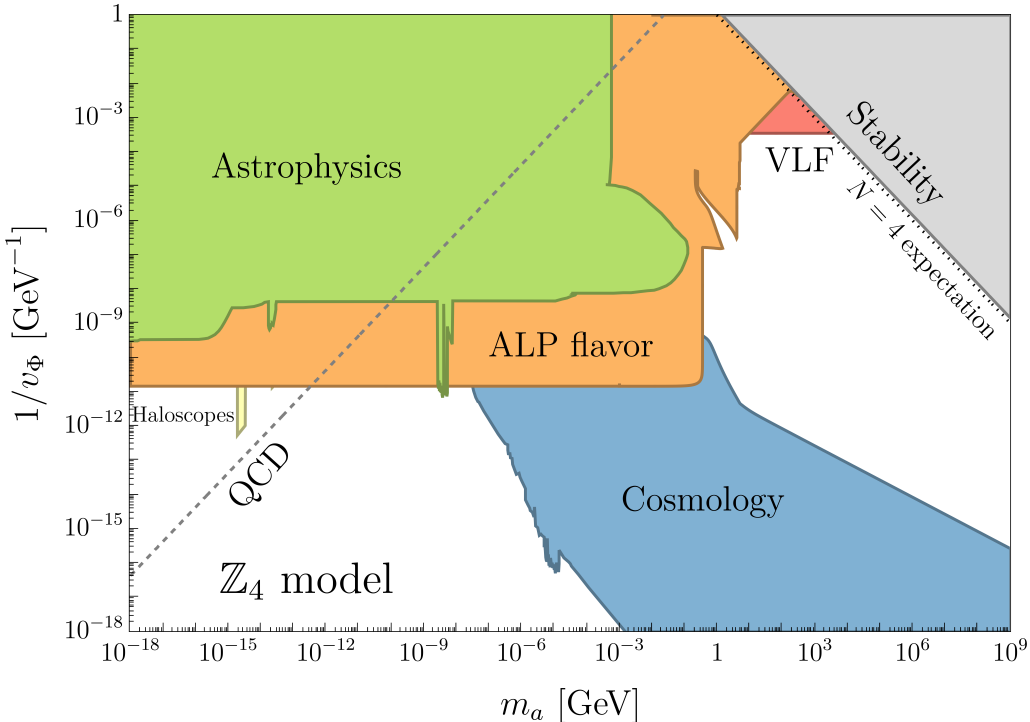


Figure 5: A global overview of the phenomenology of a FN ALP in the $(m_a, 1/v_\Phi)$ plane. The gray region is excluded by the stability of the potential, the dotted line shows the $N = 4$ expectation, and the dashed line shows the QCD expectation, as discussed around Figure 1. The rest of the contours are due to the constraints discussed in detail in Section 3.2. The red contour is due to the constraints from the UV VLFs, the orange contour is due to the combined constraints on the FN ALP from flavor observables, while the green, yellow, and blue contours are due to astrophysics, haloscopes, and cosmology, respectively. See the surrounding text for more details.

constraints depicted in green are less important in scenarios with flavorful ALPs. In blue, we show the constraints from cosmology mentioned earlier, with the left part taken from Ref. [124] and the right coming from the requirement of not spoiling the success of BBN. Although these constraints are important in a large part of the parameter space, we now *zoom in* to a region that is arguably more interesting for low-scale FN models.

In Fig. 6, we show a zoomed-in version of Fig. 5, now focusing on the ALP masses in the range $m_a \in [0.1, 10^4]$ GeV. This region of the parameter space is of main interest for the FN models studied in this work and is constrained mainly from flavor physics observables. We emphasize again that the constraint due to VLFs dominates the natural \mathbb{Z}_4 model. However, by allowing for $\lambda'_N \ll 1$ we can in principle populate the whole parameter space. Moreover, as we will see in the next section, the qualitative picture varies little, even for more elaborate \mathbb{Z}_N models. Since the ALP flavor constraints dominate a large portion of this parameter space, we now split them into multiple contours to differentiate between observables. In the subsequent discussion, we move from high to low ALP masses, commenting on the leading constraints for the different regimes.

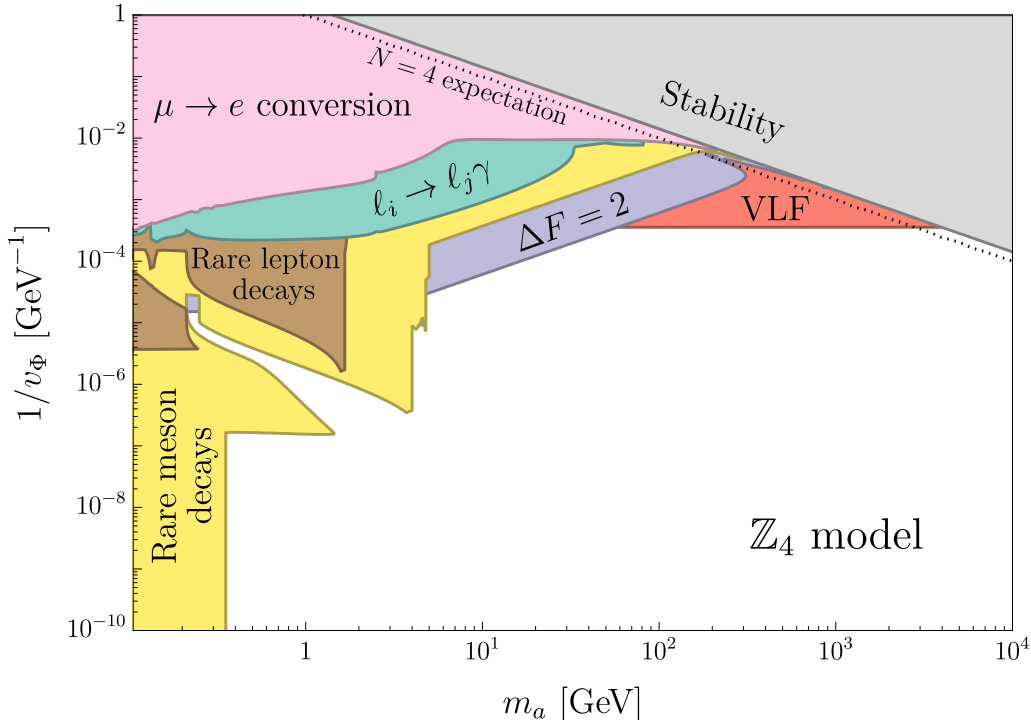


Figure 6: A zoomed-in version of Figure 5, focusing on the parameter space interesting for low-scale FN models. Again, the gray region is excluded by potential stability, while the dotted line shows the expectation of $N = 4$. We show the leading constraint from VLFs in red and a compendium of constraints on the flavorful ALP in the rest of the contours. See the surrounding text for a detailed discussion.

In purple, we show the combined constraints from the ALP contributions to neutral meson mixing observables, here dominated by ϵ_K . These provide the leading constraint for $m_B \lesssim m_a \lesssim 60$ GeV, setting $v_\Phi \gtrsim 10 - 100$ TeV. Rare meson decays become kinematically allowed for ALP masses below m_B , as depicted in the yellow contour. At first, B -meson decays to visible final states provide the leading constraint, dominated by displaced vertex analyses of $B \rightarrow K^{(*)}\mu\mu$ by LHCb, setting $v_\Phi \gtrsim 100 - 1000$ TeV. The region below that is due to $B \rightarrow Ka$, setting an upper and a lower bound on v_Φ as we demand the ALP to behave as an invisible final state, as discussed in the previous subsection. Finally, for ALP masses below m_K , $K \rightarrow \pi a$ decays completely dominate the phenomenology.

For completeness we comment on the subleading LFV phenomenology: in brown contours, we depict the combined constraints from rare lepton decays, dominated first by $\tau \rightarrow 3\mu$ and then by $\tau \rightarrow \mu + \text{invisible}$, with the flat region being associated to the plateau of $\tau \rightarrow M^{(*)}\mu$ where $M^{(*)}$ are unflavored mesons. In water green, we show the constraints from $\ell_i \rightarrow \ell_j \gamma$, with the sensitivity of up to $v_\Phi \gtrsim 10$ TeV. Finally, in pink, we show the contour from $\mu \rightarrow e$ conversion, currently setting bounds up to $v_\Phi \gtrsim$ TeV.

Looking ahead, several experimental advancements will significantly probe the allowed parameter space, see e.g. [137]. First, future bounds on charged lepton flavor violation

from μ to e conversion [138, 139] will impose stricter constraints on the UV sector, pushing the FN scale by another order of magnitude. Second, there is a pressing need for dedicated experimental programs to search for many $M \rightarrow M'a$ and $\ell \rightarrow \ell'a$ processes with displaced ALP vertices $a \rightarrow \ell_i \ell_j, \gamma\gamma$, etc. Finally, both Belle-II and LHCb will improve the existing limits on rare decays, further pushing into the unexplored territory.

4 A finer model: \mathbb{Z}_8

The simplicity of the \mathbb{Z}_4 model comes at the expense of not perfectly explaining the quark and lepton flavor hierarchies. While the existence of hierarchies between generations is consistently predicted, this model fails to account for the smallness of the bottom and tau Yukawas, which are observed to be $\mathcal{O}(0.01)$ instead of the expected $\mathcal{O}(1)$. Furthermore, the mass hierarchy between different generations of down quarks and charged leptons is more compressed compared to that of the up quarks, despite the \mathbb{Z}_4 model predicting a universal ϵ factor between generations for all three gauge representations. These additional finer features of the SM flavor puzzle call for a larger symmetry.

\mathbb{Z}_8 EFT. The up-quark sector exhibits a double hierarchy compared to the down sector. This feature was recently successfully achieved by the $U(2)_{q+e^c+u^c} \times \mathbb{Z}_2$ symmetry in Ref. [25], which retains the favorable characteristics of $U(2)_{q+e^c}$, including the neutrino anarchy, while producing a single (double) hierarchy in the down (up) quarks. The \mathbb{Z}_2 factor serves to suppress overall the down sector, which explains the smallness of $y_{b,\tau}$. This section demonstrates that the smallest discrete symmetry capable of reproducing the same texture as in Ref. [25] is \mathbb{Z}_8 .

To illustrate this, if the hierarchy parameter in the down sector is ϵ , then in the up sector, it should be ϵ^2 , leading to $y_u/y_t \sim (y_d/y_b)^2 \sim \epsilon^4$. Following the discussion below Eq. (2.1), given the largest $n_{ij}^f = 4$, the minimal symmetry group required is therefore \mathbb{Z}_8 . The non-trivially charged fields in this case are $[q_1] = -[e_3] = -[u_1] = 2$, $[q_2] = -[e_2] = -[u_2] = 1$, $[d_i] = -2$ and $[\ell_i] = 4$, where $i = 1, 2, 3$. The leading patterns are

$$n_{ij}^d = \begin{pmatrix} 4 & 4 & 4 \\ 3 & 3 & 3 \\ 2 & 2 & 2 \end{pmatrix}, \quad n_{ij}^{e'} = \begin{pmatrix} 4 & 3 & 2 \\ 4 & 3 & 2 \\ 4 & 3 & 2 \end{pmatrix}, \quad n_{ij}^u = \begin{pmatrix} 4 & 3 & 2 \\ 3 & 2 & 1 \\ 2 & 1 & 0 \end{pmatrix}, \quad (4.1)$$

while n_{ij}^d, n_{ij}^e and n_{ij}^u give comparable or subleading contributions to Y_{ij}^f .

A few comments are in order. First, we can see explicitly why the \mathbb{Z}_8 symmetry is necessary. A replacement $\Phi^M \rightarrow (\Phi^*)^{N-M}$ would disrupt the hierarchies if $N < 8$. In addition, the universal charges for d_i and ℓ_i are chosen to be different, even though they lead to the same singular values $\hat{y}_{ii}^{d,e} \sim \{\epsilon^4, \epsilon^3, \epsilon^2\}$. This choice allows the CKM matrix to be approximately a unit matrix while implying no selection rules on the neutrino sector. In other words, the Weinberg operator

$$-\mathcal{L} \supset \frac{y_{ij}^\nu}{M_\nu} \ell_i \ell_j H H, \quad (4.2)$$

is neutral under the \mathbb{Z}_8 symmetry. Therefore, it features anarchic coefficients, which is consistent with the large observed mixings in the PMNS matrix.²³

The details of fitting x_{ij}^f and $x_{ij}^{f'}$ from Eq. (2.1) to the observed SM flavor parameters are presented in Appendix A.2. As demonstrated by the numerical benchmark point, this FN EFT offers an excellent description of the SM flavor parameters for $\epsilon \simeq 6.6 \times 10^{-2}$ with all fit parameters being $\mathcal{O}(1)$, as anticipated.

UV completion. The set of VLF with masses at the scale M , completing Eq. (2.1) for the \mathbb{Z}_8 charges listed above, is somewhat more complex than in the previous section. Let us start with the quark sector. The charges of the new VLF fields are

$$\begin{aligned} [Q_2^a] &= 0, & [Q_1] &= 1, \\ [U_2^a] &= 0, & [U_1] &= -1, \\ [D_2^i] &= 0, & [D_1^i] &= -1. \end{aligned} \tag{4.3}$$

The gauge representations correspond to the SM q , u , and d fields, respectively, with $a = 1, 2$ and $i = 1, 2, 3$. Adding these states in the UV allows for the tree-level completion of the effective quark Yukawa operators. The corresponding diagrams are analogous to those in Fig. 4, featuring n_{ij}^f VLF propagators. The effective Yukawa matrix entries parametrically scale as

$$Y_{ij}^f \sim (y_*)^{n_{ij}^f+1} \epsilon^{n_{ij}^f}. \tag{4.4}$$

Here, y_* generically represents a dimension-4 coupling in the UV Lagrangian. As previously discussed, the product of several $\mathcal{O}(0.3)$ couplings can contribute to hierarchies. Consequently, we expect the variance in the UV couplings to be even smaller than in the EFT fit presented above, similar to what was observed for the \mathbb{Z}_4 model.

Let us now turn our discussion to the charged lepton sector. The required set of VLF, all in the gauge representation of the SM field ℓ , is

$$[L_N] = 0, \quad [L_{N-1}^a] = -1, \quad [L_{N-2}^i] = -2, \quad [L_{N-3}^i] = -3, \tag{4.5}$$

where $N = 8$. Integrating them out at the tree level produces the desired charged lepton effective Yukawa operators. An example diagram involves connecting e_1 (which has charge zero) with ℓ_i (charge 4) through the aforementioned chain of VLF, attaching H , and subsequently adding four Φ^* .

The final model-building task is to endow the ALP with a non-null mass. The simplest option is to consider the wheel diagram already introduced in Fig. 2, which requires a full set of VLF representation charges. Since we already have half of the L_k charges, we only

²³In the type-I seesaw scenario, completing this operator with heavy right-handed neutrinos ν_i means $[\nu_i] = 4$, ensuring that both the Yukawa interaction and Majorana mass terms are allowed by the \mathbb{Z}_8 symmetry.

need, in addition,²⁴

$$[L_1] = 1, \quad [L_2] = 2, \quad [L_3] = 3, \quad [L_4] = 4, \quad (4.6)$$

which together with Eq. (4.5) gives the diagram in Fig. 2. The prediction for the ALP mass aligns precisely with the one discussed in Section 2 for the $N = 8$ case, as shown in Fig. 1. We expect $m_a/v_\Phi \sim \{10^{-6}, 10^{-4}\}$, see Eq. (2.9) and the discussion below it. Thus, unlike in the \mathbb{Z}_4 model, here we expect a light ALP, potentially leading to interesting effects described by the SM+ a EFT.

Phenomenology. First, let us discuss the UV contributions to operators without Φ insertions before moving on to the ALP.

VLF. The leading effect arises from $\mathcal{L} \supset y_{D_1}^{ij} \bar{D}_1^i \Phi d^j$, which, after integrating out D_1^i at the one-loop level, matches to the $(\bar{d}_1 \gamma_\mu d_2)^2$ operator. This is analogous to the \mathbb{Z}_4 model, where the H and Q_2^1 fields appeared in the box diagram, whereas in this case, we have the Φ and D_1^i fields (see Eq. (3.27) and the subsequent discussion). Therefore, the leading constraint comes from ϵ_K and can be easily derived by rescaling the \mathbb{Z}_4 case by the ϵ ratios in the two models. Since ϵ is larger in the \mathbb{Z}_8 model, the bound becomes $v_\Phi \gtrsim 40$ TeV, up to $\mathcal{O}(1)$ variation in $y_{D_1}^{ij}$.

ALP. Assuming v_Φ saturates this bound, we expect $m_a \in (0.04, 4)$ GeV. This mass range coincides with numerous significant flavor constraints in the \mathbb{Z}_4 model, providing leading bounds on the FN scale. We first need to examine the ALP coupling matrices to compare the predictions between the two models. In this case, the hierarchies in the left-handed rotation matrices U_L^d and U_L^u are similar. Hence, the CKM receives, in principle, a sizeable contribution from both. Furthermore, this case has many more free parameters for Y_u . For this reason, we find it more instructive to report the general structure of the couplings in the \mathbb{Z}_8 model up to $\mathcal{O}(1)$ factors:

$$c^d \sim \begin{pmatrix} m_d & m_s \frac{m_d}{m_s} & m_b \frac{m_d}{m_b} \\ m_d \frac{m_d}{m_s} & m_s & m_b \frac{m_s}{m_b} \\ m_d \frac{m_d}{m_b} & m_s \frac{m_s}{m_b} & m_b \end{pmatrix}, \quad c^u \sim \begin{pmatrix} m_u & m_c \sqrt{\frac{m_u}{m_c}} & m_t \sqrt{\frac{m_u}{m_t}} \\ m_c \sqrt{\frac{m_u}{m_c}} & m_c & m_t \sqrt{\frac{m_c}{m_t}} \\ m_t \sqrt{\frac{m_u}{m_t}} & m_t \sqrt{\frac{m_c}{m_t}} & m_t \frac{m_c}{m_t} \end{pmatrix}, \quad (4.7)$$

$$c^e \sim \begin{pmatrix} m_e & m_e \frac{m_e}{m_\mu} & m_e \frac{m_e}{m_\tau} \\ m_\mu \frac{m_e}{m_\mu} & m_\mu & m_\mu \frac{m_\mu}{m_\tau} \\ m_\tau \frac{m_e}{m_\tau} & m_\tau \frac{m_\mu}{m_\tau} & m_\tau \end{pmatrix}.$$

The most prominent differences compared to the \mathbb{Z}_4 case are c_{33}^e, c_{33}^d , which now are unsuppressed due to the fact that the third generation is charged, and of course, the whole c^u . The fact that c^u mixings scale as the square root of the ratios of masses is due to the fact that neither q_i nor u_i are “universally” charged, unlike d_i and e_i . In comparison with the latter two, the up sector has doubled suppression. Hence, the mixings are “split”

²⁴Due to the large number of $SU(2)_L$ doublets in this model, the gauge coupling g_2 develops a Landau pole at approximately 10^{14} GeV for $M = 1$ PeV (1-loop estimate). In contrast, for the \mathbb{Z}_4 model, the couplings remain perturbative up to the Planck scale.

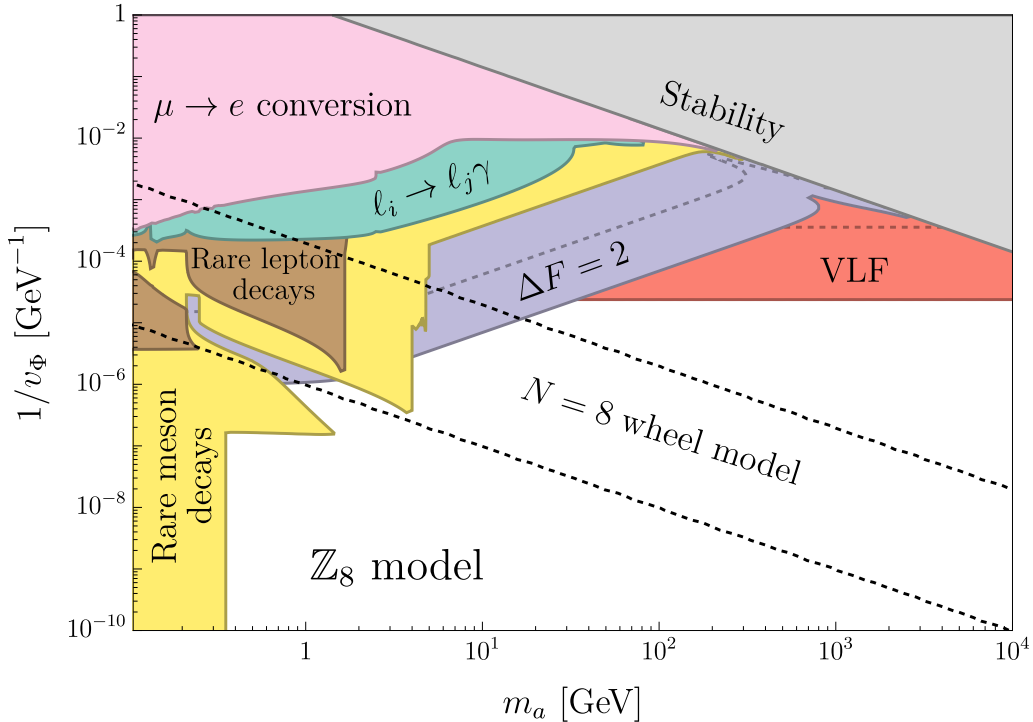


Figure 7: Constraints in the $(m_a, 1/v_\Phi)$ plane, similar to Figure 6, but now for the \mathbb{Z}_8 model. The gray region is excluded by vacuum stability, while the dashed black lines show the expected range in a $N = 8$ wheel model. The red and purple (full) contours show the major differences with respect to the \mathbb{Z}_4 case (dashed). The rest of the constraints are qualitatively the same as in the \mathbb{Z}_4 case. See the surrounding text for more details.

between the left and right rotation matrices, which give comparable contributions to c^u , see Eq. (B.10). Because of this, ALP contributions to $D - \bar{D}$ mixing become now more important [140]. In particular, if the CKM matrix is still fully given by U_L^d , as is for simplicity assumed in the example of App. A.2, the constraint from \mathbb{Z}_4 due to ϵ_K remains essentially the same. Hence, in this case, CP violation in D meson mixing is actually the most important $\Delta F = 2$ probe. In the general case in which the CKM receives sizeable contributions from both the diagonalizing matrices, we find that the ϵ_K bound becomes slightly stronger than in the \mathbb{Z}_4 case, leading to bounds comparable to that from CP violation in $D - \bar{D}$ mixing.

We illustrate the phenomenology of the \mathbb{Z}_8 model in Figure 7. The dashed black lines now show the expectation in the $(m_a, 1/v_\Phi)$ plane for a $N = 8$ wheel model, as already discussed around Figure 1. With dashed red and purple lines we show the $\Delta F = 2$ and VLF constraints in the case of \mathbb{Z}_4 , as in Figure 6. The full contours show the respective bounds in the \mathbb{Z}_8 case, both stronger in line with the discussion above. It is interesting to note how in this scenario, contrary to the case of \mathbb{Z}_4 , the leading phenomenology is due to the light flavorful ALP and no longer due to the VLFs. In particular, the $\Delta F = 2$ constraints together with displaced vertex searches in $B \rightarrow K^{(*)}\mu\mu$ (quantitatively the

same as in \mathbb{Z}_4), set the most stringent constraints of order $v_\Phi \gtrsim 10^5 - 10^7$ GeV for the corresponding expected mass range of $m_a \in [1, 20]$ GeV.

5 Conclusion

The presence of an ALP in quark and lepton flavor physics opens up a diverse array of new phenomena, making it an exciting area of research for phenomenologists. The appropriate theoretical framework to study these effects is the SM+ a EFT, which constructs a tower of local operators that respect both the SM symmetry and the approximate ALP shift symmetry. However, depending on the coefficients of the operators and the ALP mass, which are input parameters a priori, the expected patterns of deviations vary widely, thereby reducing the predictive power of this approach.

In the bulk of this paper, we surveyed the flavor physics phenomenology in the presence of an ALP, adding, however, a deeper UV context to the study. Specifically, we imposed a discrete FN symmetry motivated by the SM flavor puzzle. This symmetry provides power counting and selection rules that correlate various observables, offering a structured and focused framework for studying ALP effects in flavor physics. The main results are summarized in Figures 6 and 7, which depict the parameter space of the ALP mass versus the FN scale. The two plots interpret a plethora of flavor physics measurements discussed in Section 3.2, organized into suitable categories, within two concrete models based on \mathbb{Z}_4 and \mathbb{Z}_8 FN symmetries, respectively. The two choices allow us to quantify the uncertainty due to variations in the realization of the FN mechanism.

Prior to the comprehensive phenomenological work, we introduced a whole class of FN models based on \mathbb{Z}_N symmetries. While a commonly considered perturbatively-exact $U(1)_{\text{FN}}$ predicts a very light (pseudo) Goldstone boson, the advantage of the discrete symmetries is that m_a can be considerably heavier, opening up new phenomenological possibilities as discussed above. We began in Section 2 by charting the ALP parameter space based on theoretical considerations, as summarized in Fig. 1, and by presenting concrete predictive models, such as the wheel model shown in Fig. 2. This setup is more predictive than an explicitly broken $U(1)_{\text{FN}}$, which can produce correct textures provided $m_a \lesssim v_\Phi$ but does not correlate the two parameters. Nevertheless, our results qualitatively apply to the latter case as well. Assuming marginal couplings of $\mathcal{O}(1)$, our models predict a region in (m_a, v_Φ) as illustrated in the plots for the two chosen examples. Notably, the \mathbb{Z}_4 model is unique in predicting $m_a \sim v_\Phi$ due to the presence of a $U(1)_{\text{FN}}$ -breaking dimension-4 term in the potential.

Another advantage of the \mathbb{Z}_N class is the ability to balance between simplicity versus “baroqueness”, controlled by the value of N . Unsurprisingly, a large enough N allows for a perfect fit of the SM flavor parameters. However, we prioritized simplicity, accepting an increased variance in the UV parameters. Following this path, we uncovered a remarkably simple and elegant model based on the \mathbb{Z}_4 group (Section 3.1). By charging only left-handed quarks and right-handed charged leptons, this model generates hierarchies in the charged fermion masses and left-handed quark mixing matrices while maintaining an anarchic neutrino flavor structure. This minimal symmetry framework produces similar

Yukawa textures as the full $U(2)_{q+e}$ symmetry recently proposed in [25]. To address subtleties of the SM flavor puzzle, such as the smallness of $y_{b,\tau}$ and the difference in up versus down quark mass hierarchies, we introduced a refined \mathbb{Z}_8 model in Section 4. This model is carefully crafted, drawing inspiration from the novel $U(2)_{q+e^c+u^c} \times \mathbb{Z}_2$ symmetry proposed recently in [25].

A crucial aspect of our work is that in both scenarios, we constructed explicit renormalizable completions featuring new vector-like fermions with masses above the FN scale, given by v_Φ/ϵ where ϵ is the FN spurion controlling the Yukawa textures. These new fields generate effective Yukawa operators in Eq. (2.1), but can also lead to deviations in rare flavor-changing neutral currents. An intriguing question arises about how the constraints on the minimal UV sector, which is essential for completing the FN mechanism, compare to those from a light ALP. The explicit models provide a basis for conducting precision calculations and studying this interplay between the ALP and the irreducible UV-induced effects. The so-called VLF bounds, shown in red in Figures 6 and 7, are dominant for a heavy ALP ($m_a \gtrsim 100$ GeV). This parameter space region permits the lowest FN scale v_Φ . For instance, in the case of \mathbb{Z}_4 predicting $m_a \sim v_\Phi$, the FN symmetry could be restored even at the TeV scale.

In conclusion, with its rich phenomenology and solid theoretical foundations, the FN ALP represents an exciting physics frontier for ongoing and future experiments in flavor and collider physics.

Acknowledgments

This work received funding from the Swiss National Science Foundation (SNF) through the Eccellenza Professorial Fellowship, project number 186866, ‘‘Flavor Physics at the High Energy Frontier.’’

A UV and EFT parameters matching

A.1 \mathbb{Z}_4 model

A.1.1 EFT

In the \mathbb{Z}_4 model, other than Φ , only q_i and e_i are charged under the flavor symmetry, with charges $[q_1] = -[e_1] = 2$, $[q_2] = -[e_2] = 1$. Hence, one can always perform a set of unitary rotations of u_i, d_i, ℓ_i such that the SM Yukawas read, after Φ condensation,

$$Y_d = \begin{pmatrix} z_{d_1}\epsilon^2 & z_{d_2}\epsilon^2 & z_{d_3}\epsilon^2 \\ 0 & y_{d_2}\epsilon & y_{d_3}\epsilon \\ 0 & 0 & x_{d_3} \end{pmatrix}, \quad Y_u = \begin{pmatrix} z_{u_1}\epsilon^2 & z_{u_2}\epsilon^2 & z_{u_3}\epsilon^2 \\ 0 & y_{u_2}\epsilon & y_{u_3}\epsilon \\ 0 & 0 & x_{u_3} \end{pmatrix}, \quad Y_e = \begin{pmatrix} z_{e_1}\epsilon^2 & 0 & 0 \\ z_{e_2}\epsilon^2 & y_{e_2}\epsilon & 0 \\ z_{e_3}\epsilon^2 & y_{e_3}\epsilon & x_{e_3} \end{pmatrix}, \quad (\text{A.1})$$

with $\epsilon \equiv v_\Phi/\sqrt{2}M$. The parameters in Eq. (A.1) correspond to x_{ij}^f in Eq. (2.1) and exploiting the residual rephasing symmetry of the SM fields can all be made real, except five of them which we take to be $z_{d_3}, z_{u_2}, z_{u_3}, y_{u_3}$ and z_{e_3} . A perturbative singular value

decomposition of Eq. (A.1) reveals that the SM Yukawa matrices in the mass basis are simply given by the diagonal elements,

$$\begin{aligned} (y_d, y_s, y_b) &\simeq (z_{d_1}\epsilon^2, y_{d_2}\epsilon, x_{d_3}), \\ (y_u, y_c, y_t) &\simeq (z_{u_1}\epsilon^2, y_{u_2}\epsilon, x_{u_3}), \\ (y_e, y_\mu, y_\tau) &\simeq (z_{e_1}\epsilon^2, y_{e_2}\epsilon, x_{e_3}), \end{aligned} \quad (\text{A.2})$$

with the leading rotation matrices

$$U_L^d \simeq \begin{pmatrix} 1 & \frac{z_{d_2}}{y_{d_2}}\epsilon & \frac{z_{d_3}}{x_{d_3}}\epsilon^2 \\ -\frac{z_{d_2}}{y_{d_2}}\epsilon & 1 & \frac{y_{d_3}}{x_{d_3}}\epsilon \\ \frac{y_{d_3}z_{d_2}-y_{d_2}z_{d_3}^*}{x_{d_3}y_{d_2}}\epsilon^2 & -\frac{y_{d_3}}{x_{d_3}}\epsilon & 1 \end{pmatrix} \simeq \begin{pmatrix} 1 & \frac{m_d}{m_s}\frac{z_{d_2}}{z_{d_1}} & \frac{m_d}{m_b}\frac{z_{d_3}}{z_{d_1}} \\ -\frac{m_d}{m_s}\frac{z_{d_2}}{z_{d_1}} & 1 & \frac{m_s}{m_b}\frac{y_{d_3}}{y_{d_2}} \\ \frac{m_d}{m_b}\frac{y_{d_3}z_{d_2}-y_{d_2}z_{d_3}^*}{y_{d_2}z_{d_1}} & -\frac{m_s}{m_b}\frac{y_{d_3}}{y_{d_2}} & 1 \end{pmatrix}, \quad (\text{A.3})$$

and similarly for U_L^u and $(U_R^e)^*$. The Eq. (A.3) shows that for $\mathcal{O}(1)$ parameters, the CKM mixings can be reproduced quite well, and clarifies why in Sec. 3 we assumed $V_{\text{CKM}} \simeq U_L^d$: the bigger hierarchies in the up sector suppress the off-diagonal entries of U_L^u to the point that a significant fine-tuning would be required for it to actually contribute to V_{CKM} .

Eqs. (A.2) and (A.3) can be used to fix some of the parameters in Eq. (A.1), including ϵ . The optimal benchmark, where the parameters are close to $\mathcal{O}(1)$ and which is used to derive the bounds in the main text, is achieved for $\epsilon \approx 4.4 \times 10^{-3}$ with

$$\begin{aligned} Y_d &\simeq \begin{pmatrix} 0.55\epsilon^2 & 2.5\epsilon^2 & (0.73 - 1.8i)\epsilon^2 \\ 0 & 0.049\epsilon & 0.10\epsilon \\ 0 & 0 & 0.011 \end{pmatrix}, & Y_u &\simeq \begin{pmatrix} 0.25\epsilon^2 & z_{u_2}\epsilon^2 & z_{u_3}\epsilon^2 \\ 0 & 0.57\epsilon & y_{u_3}\epsilon \\ 0 & 0 & 0.71 \end{pmatrix}, \\ Y_e &\simeq \begin{pmatrix} 0.15\epsilon^2 & 0 & 0 \\ z_{e_2}\epsilon & 0.14\epsilon & 0 \\ z_{e_3} & y_{e_3} & 0.01 \end{pmatrix}. \end{aligned} \quad (\text{A.4})$$

where for the fit, we used the value of the SM Yukawas at 100 TeV from [141]. The presence of some $\mathcal{O}(10^{-1})$ hierarchies in the lighter generations is not a problem, as it can naturally be explained by a product of several UV couplings of order $\mathcal{O}(0.3)$. Conversely, the small values of the bottom and tau Yukawas, approximately $\mathcal{O}(10^{-2})$, as indicated by x_{d_3} and x_{e_3} , cannot be accounted for within this model and must be accepted as given.

A.1.2 UV

Integrating out the VLF in Eq. (3.1) at tree-level leads to a FN EFT with Yukawas

$$Y^{(u,d)} = \begin{pmatrix} \epsilon_Q^2 r_Q x_1^q x_{12}^{qa} \mathbf{y}^{(u,d)a} \\ \epsilon_Q x_2^{qa} \mathbf{y}^{(u,d)a} \\ \mathbf{z}^{(u,d)} \end{pmatrix}, \quad Y^e = \begin{pmatrix} \epsilon_E^2 r_E x_1^e x_{12}^{ea} \mathbf{y}^{ea} & \epsilon_E x_2^{ea} \mathbf{y}^{ea} & \mathbf{z}^{eT} \end{pmatrix}, \quad (\text{A.5})$$

where $\epsilon_Q \equiv v_\Phi/\sqrt{2}M_{Q_2}$, $\epsilon_E \equiv v_\Phi/\sqrt{2}M_{E_2}$. For simplicity, we have assumed degenerate Q_2^a and E_2^a masses and $r_Q = M_{Q_2}/M_{Q_1}$, $r_E = M_{E_2}/M_{E_1}$. Boldface quantities denote vectors

in flavor space. To match Eq. (A.5) to (A.1) and ultimately the SM masses and mixings, it is convenient to pick a basis in the UV theory, which simplifies calculation as much as possible. Rotation of the fields in Eq. (3.1) allows us to put the couplings in the following schematic form

$$\begin{aligned}
M_{Q_1} &\sim \mathbb{R}, & M_{Q_2} &\sim \text{diag}(\mathbb{R}, \mathbb{R}), & M_{E_1} &\sim \mathbb{R}, & M_{E_2} &\sim \text{diag}(\mathbb{R}, \mathbb{R}), \\
z_d &\sim (0, 0, \mathbb{R}), & z_u &\sim (0, 0, \mathbb{R}), & z_e &\sim (0, 0, \mathbb{R}), \\
\mathbf{y}^{da} &\sim \begin{pmatrix} \mathbb{R} & \mathbb{C} & \mathbb{C} \\ 0 & \mathbb{R} & \mathbb{R} \end{pmatrix}, & \mathbf{y}^{ua} &\sim \begin{pmatrix} \mathbb{R} & \mathbb{C} & \mathbb{C} \\ 0 & \mathbb{R} & \mathbb{C} \end{pmatrix}, & \mathbf{y}^{ea} &\sim \begin{pmatrix} 0 & \mathbb{R} \\ \mathbb{R} & \mathbb{C} \\ \mathbb{R} & \mathbb{C} \end{pmatrix}, \\
x_2^{qa} &\sim (0, \mathbb{R}), & x_{12}^{qa} &\sim (\mathbb{R}, \mathbb{C}), & x_1^q &\sim \mathbb{R}, \\
x_2^{ea} &\sim (\mathbb{R}, 0), & x_{12}^{ea} &\sim (\mathbb{R}, \mathbb{R}), & x_1^e &\sim \mathbb{R},
\end{aligned} \tag{A.6}$$

which leads to Yukawas with the triangular structure of (A.1). Unfortunately, the matching is still not straightforward as not all the phases in (A.6) are physical in the EFT. A spurious phase in $\delta^d = \arg(Y_d)_{12}$ must be removed with the rotation $d_{2,3} \rightarrow e^{-i\delta^d} d_{2,3}$, $\bar{q}_{2,3} \rightarrow e^{i\delta^d} \bar{q}_{2,3}$, $u_{2,3} \rightarrow e^{-i\delta^d} u_{2,3}$ and must be taken into account when matching the UV parameters to (A.2), (A.3). Note that this rotation also affects the off-diagonal entries of Y_u (unfixed in the EFT) and the Wilson coefficient of higher-dimensional operators in a non-trivial manner. Similarly, a spurious phase δ^e in $(Y_e)_{21}$ also appears, which can be removed with $\bar{\ell}_{2,3} \rightarrow \bar{\ell}_{2,3} e^{-i\delta^e}$, $e_{2,3} \rightarrow e_{2,3} e^{i\delta^e}$.

The matching conditions for the down and quarks and the leptons read:

$$\left\{ \begin{aligned}
r_Q x_1^q x_{12}^{q1} y_1^{d1} &= z_{d1} = \hat{y}_d / \epsilon^2 \\
x_2^{q2} y_2^{d2} &= y_{d2} = \hat{y}_s / \epsilon \\
x_2^{q2} y_3^{d2} &= y_{d3} = A \lambda_c^2 \hat{y}_b / \epsilon \\
r_Q x_1^q [x_{12}^{q1} y_2^{d1} + x_{12}^{q2} y_2^{d2}] &= \rho_d e^{i\delta_d}, & \rho_d &= z_{d2} = \lambda_c y_{d2} / \epsilon = \lambda_c \hat{y}_s / \epsilon^2 \\
r_Q x_1^q [x_{12}^{q1} y_3^{d1} + x_{12}^{q2} y_3^{d2}] e^{-i\delta_d} &= z_{d3} = A \lambda_c^3 (\rho - i\eta) \hat{y}_b / \epsilon^2
\end{aligned} \right. \tag{down quarks}, \tag{A.7}$$

$$\left\{ \begin{aligned}
r_Q x_1^q x_{12}^{q1} y_1^{u1} &= z_{u1} = \hat{y}_u / \epsilon^2 \\
x_2^{q2} y_2^{u2} &= y_{u2} = \hat{y}_c / \epsilon \\
x_2^{q2} y_3^{u2} &= y_{u3} \\
r_Q x_1^q [x_{12}^{q1} y_2^{u1} + x_{12}^{q2} y_2^{u2}] e^{-i\delta^d} &= z_{u2} \\
r_Q x_1^q [x_{12}^{q1} y_3^{u1} + x_{12}^{q2} y_3^{u2}] e^{-i\delta^d} &= z_{u3}
\end{aligned} \right. \tag{up quarks}, \tag{A.8}$$

$$\left\{ \begin{array}{l} r_E x_1^e x_{12}^{e2} y_1^{e2} = z_{e_1} = \hat{y}_e / \epsilon^2 \\ x_2^{e1} y_2^{e1} = y_{e_2} = \hat{y}_\mu / \epsilon \\ x_2^{e1} y_3^{e1} = y_{e_3} \\ r_E x_1^e [x_{12}^{e2} y_2^{e2} + x_{12}^{e1} y_2^{e1}] = \rho_e e^{i\delta^e}, \quad \rho_e = z_{e_2} \\ r_E x_1^e [x_{12}^{e2} y_3^{e2} + x_{12}^{e1} y_3^{e1}] e^{-i\delta^e} = z_{e_3} \end{array} \right. \quad (\text{leptons}). \quad (\text{A.9})$$

The solution to this system of equations is clearly not unique. Unfortunately, we were not able to completely solve this system analytically due to the last two equations in (A.7), which involve non-polynomial functions of the UV parameters and can be expressed as

$$\left\{ \begin{array}{l} |x_2 + z| = b \\ |x_3 + az| = d \\ \arg[x_3 + az] - \arg[x_2 + z] = c \end{array} \right. \quad (\text{A.10})$$

where $a = A\lambda_c^2 \hat{y}_b / \hat{y}_s$, $b = \lambda_c \hat{y}_s / \hat{y}_d$, $c = \arg A\lambda_c^3 (\rho - i\eta)$ and $d = |A\lambda_c^3 (\rho - i\eta)| \hat{y}_b / \hat{y}_d$, and we introduced the combinations $x_2 = y_2^{d1} / y_1^{d1}$, $x_3 = y_3^{d1} / y_1^{d1}$, $z = x_{12}^{q2} y_2^{q2} / (x_{12}^{q1} y_1^{q1})$. To derive the bounds in Section 3, we pick a representative benchmark obtained by numerically solving (A.10) (again, solutions are not unique) and choosing the remaining parameters in such a way to reproduce (A.4). This reads for the quarks

$$\begin{aligned} \mathbf{z}_d &= (0, 0, y_b), \quad \mathbf{z}_t = (0, 0, y_t), \\ \mathbf{y}^{da} &= \begin{pmatrix} 0.26 & -0.28 - 0.96i & -0.95 + 0.24i \\ 0 & 0.10 & 0.21 \end{pmatrix}, \quad \mathbf{y}^{ua} = \begin{pmatrix} 0.12 & -0.57 - 0.20i & 0.24 + 0.16i \\ 0 & 1.2 & -0.86 + 0.14i \end{pmatrix}, \\ r_Q &= 4, \quad x_1^q = 0.96, \quad x_2^{qa} = (0, 0.47), \quad x_{12}^{qa} = (0.55, 0.07 - 0.99i), \end{aligned} \quad (\text{A.11})$$

and for the leptons

$$\begin{aligned} \mathbf{z}_e &= (0, 0, y_\tau), \\ \mathbf{y}^{ea} &= \begin{pmatrix} 0 & 0.69 \\ 0.38 & 0.47 + 0.23i \\ 0.49 & 0.19 + 0.52i \end{pmatrix}, \\ r_E &= 0.5, \quad x_2^{ea} = (0.39, 0), \quad x_{12}^{ea} = (0.45, 0.54), \quad x_1^e = 0.8. \end{aligned} \quad (\text{A.12})$$

with $\delta^d = -1.2$ and $\delta^e = 0.28$. This benchmark fixes the remaining entries of (A.5), after the δ^d, δ^u rotation, to $z_{e_2} = 0.18$, $z_{e_3} = 0.15 + 0.07i$, $y_{e_3} = 0.19$ and $z_{u_2} = 2.3 + 0.06i$, $z_{u_3} = -2.1 + 0.56i$, $y_{u_3} = -0.42 + 0.07i$.

A.2 \mathbb{Z}_8 model

In this case, with flavor rotations, we can put the Yukawa matrices in the form

$$Y_d = \begin{pmatrix} z_{d_1}\epsilon^4 & z_{d_2}\epsilon^4 & z_{d_3}\epsilon^4 \\ 0 & y_{d_2}\epsilon^3 & y_{d_3}\epsilon^3 \\ 0 & 0 & x_{d_3}\epsilon^2 \end{pmatrix}, \quad Y_u = \begin{pmatrix} z_{u_1}\epsilon^4 & z_{u_2}\epsilon^3 & z_{u_3}\epsilon^2 \\ y_{u_1}\epsilon^3 & y_{u_2}\epsilon^2 & y_{u_3}\epsilon \\ x_{u_1}\epsilon^2 & x_{u_2}\epsilon & x_{u_3} \end{pmatrix}, \quad Y_e = \begin{pmatrix} z_{e_1}\epsilon^4 & 0 & 0 \\ z_{e_2}\epsilon^4 & y_{e_2}\epsilon^3 & 0 \\ z_{e_3}\epsilon^4 & y_{e_3}\epsilon^3 & x_{e_3}\epsilon^2 \end{pmatrix}, \quad (\text{A.13})$$

where in Y_d and Y_e the only complex entries are z_{d_3} and z_{e_3} , while in Y_u all entries are complex except the diagonal ones. Assuming for simplicity that the off-diagonal entries of Y_u are small, the SM Yukawas in the mass basis are given as

$$\begin{aligned} (y_d, y_s, y_b) &\simeq (z_{d_1}\epsilon^4, y_{d_2}\epsilon^3, x_{d_3}\epsilon^2), \\ (y_u, y_c, y_t) &\simeq (z_{u_1}\epsilon^4, y_{u_2}\epsilon^2, x_{u_3}), \\ (y_e, y_\mu, y_\tau) &\simeq (z_{e_1}\epsilon^4, y_{e_2}\epsilon^3, x_{e_3}\epsilon^2), \end{aligned} \quad (\text{A.14})$$

with the CKM matrix still given by Eq. (A.3). We find that the best benchmark in this case is given by $\epsilon \simeq 6.6 \times 10^{-2}$, leading to

$$\begin{aligned} Y_d &\simeq \begin{pmatrix} 0.55\epsilon^4 & 2.5\epsilon^4 & (0.73 - 1.84i)\epsilon^4 \\ 0 & 0.74\epsilon^3 & 1.51\epsilon^3 \\ 0 & 0 & 2.4\epsilon^2 \end{pmatrix}, \quad Y_u \simeq \begin{pmatrix} 0.25\epsilon^4 & z_{u_2}\epsilon^3 & z_{u_3}\epsilon^2 \\ y_{u_1}\epsilon^3 & 0.57\epsilon^2 & y_{u_3}\epsilon \\ x_{u_1}\epsilon^2 & x_{u_2}\epsilon & 0.71 \end{pmatrix}, \\ Y_e &\simeq \begin{pmatrix} 0.15\epsilon^4 & 0 & 0 \\ z_{e_2}\epsilon^3 & 2.1\epsilon^3 & 0 \\ z_{e_3}\epsilon^2 & y_{e_3}\epsilon^2 & 2.3\epsilon^2 \end{pmatrix}. \end{aligned} \quad (\text{A.15})$$

Compared to Eq. (A.1) the fit in this case is better in terms of the parameters being close to $\mathcal{O}(1)$, with a maximum spread between the smallest and the biggest ones of $\mathcal{O}(10)$.

B Derivation of the ALP couplings

Assuming a generic Yukawa Lagrangian

$$\mathcal{L} \supset -y_{ij}^f \left(\frac{\Phi}{M} \right)^{n_{ij}^f} \bar{F}_i H f_j + \text{h.c.}, \quad (\text{B.1})$$

where F is a left-handed $\text{SU}(2)_L$ doublet and f is a right-handed singlet, we now compute the ρ and a couplings to the fermions. After SSB, we write

$$\Phi = \left(\frac{v_\Phi + \rho}{\sqrt{2}} \right) e^{ia/v_\Phi}, \quad H = \begin{pmatrix} 0 \\ \frac{v_{\text{EW}} + h}{\sqrt{2}} \end{pmatrix}. \quad (\text{B.2})$$

Plugging this into the Lagrangian above and expanding the obtained expression to leading order in ρ/v_Φ and a/v_Φ , we obtain

$$\mathcal{L} \supset -y_{ij}^f \left(\frac{v_\Phi}{\sqrt{2}M} \right)^{n_{ij}^f} \left(1 + n_{ij}^f \frac{\rho + ia}{v_\Phi} \right) \bar{f}_{Li} \left(\frac{v_{EW} + h}{\sqrt{2}} \right) f_{Rj} + \text{h.c.} + \text{h.o.} . \quad (\text{B.3})$$

where f_L is the appropriate component from the doublet F . For up-type quarks, \tilde{H} would be used instead. We define the FN expansion parameter and the fermion mass matrices

$$\epsilon = \frac{v_\Phi}{\sqrt{2}M}, \quad m_{ij}^f = \frac{v_{EW}}{\sqrt{2}} y_{ij}^f \epsilon^{n_{ij}^f}, \quad (\text{B.4})$$

seeing the FN mechanism at work once again. With this, we can write the Lagrangian as

$$\mathcal{L} \supset - \sum_{f=u,d,e} \left[m_{ij}^f \bar{f}_{Li} \left(1 + \frac{h}{v_{EW}} \right) f_{Rj} + \frac{m_{ij}^f n_{ij}^f}{v_\Phi} \bar{f}_{Li} (\rho + ia) f_{Rj} \right] + \text{h.c.} . \quad (\text{B.5})$$

Next, the fermion masses should be diagonalized as usual

$$f_R \rightarrow U_R^f f_R, \quad f_L \rightarrow U_L^f f_L, \quad U_L^{f\dagger} m^f U_R^f = \hat{m}^f, \quad (\text{B.6})$$

where \hat{m}^f is a diagonal matrix, $\hat{m}_{ij}^f \equiv m_i^f \delta_{ij}$. With this, the Higgs-Yukawa couplings are also diagonalized, whereas the a and ρ couplings are not. This induces, in general, flavor-changing neutral currents. We then have in the fermion mass basis

$$\mathcal{L} \supset - \sum_{f=u,d,e} \left[m_i^f \bar{f}_{Li} \left(1 + \frac{h}{v_{EW}} \right) f_{Ri} + c_{ij}^f \bar{f}_{Li} (\rho + ia) f_{Rj} \right] + \text{h.c.} . \quad (\text{B.7})$$

with

$$c_{ij}^f = \frac{1}{v_\Phi} (U_L^{f\dagger})_{ia} m_{ab}^f n_{ab}^f U_{Rbj}^f . \quad (\text{B.8})$$

We can further rewrite this by noting that $n_{ab}^f = [F_a] - [f_b]$ is a matrix built from (integer) FN charges. By defining diagonal charge matrices $Q_{ij}^f \equiv [f_i] \delta_{ij}$, the combination of matrices appearing in the middle can be expressed as

$$m_{ab}^f n_{ab}^f = (Q^F m^f - m^f Q^f)_{ab} . \quad (\text{B.9})$$

With this, the c^f coupling matrices can be expressed as

$$\begin{aligned} c^f &= \frac{1}{v_\Phi} \left[U_L^{f\dagger} \left(Q^F m^f - m^f Q^f \right) U_R^f \right] \\ &= \frac{1}{v_\Phi} \left[U_L^{f\dagger} Q^F \left(U_L^f U_L^{f\dagger} \right) m^f U_R^f - U_L^{f\dagger} m^f \left(U_R^f U_R^{f\dagger} \right) Q^f U_R^f \right] \\ &= \frac{1}{v_\Phi} \left[\left(U_L^{f\dagger} Q^F U_L^f \right) \hat{m}^f - \hat{m}^f \left(U_R^{f\dagger} Q^f U_R^f \right) \right] . \end{aligned} \quad (\text{B.10})$$

It is worth reemphasizing that this is now expressed in terms of diagonal fermion mass matrices \hat{m}^f and diagonal FN charge matrices Q^F and Q^f for the SU(2) doublet and singlet, respectively.

References

- [1] N. Cabibbo, *Unitary Symmetry and Leptonic Decays*, *Phys. Rev. Lett.* **10** (1963) 531.
- [2] M. Kobayashi and T. Maskawa, *CP Violation in the Renormalizable Theory of Weak Interaction*, *Prog. Theor. Phys.* **49** (1973) 652.
- [3] C.D. Froggatt and H.B. Nielsen, *Hierarchy of Quark Masses, Cabibbo Angles and CP Violation*, *Nucl. Phys. B* **147** (1979) 277.
- [4] M. Leurer, Y. Nir and N. Seiberg, *Mass matrix models*, *Nucl. Phys. B* **398** (1993) 319 [[hep-ph/9212278](#)].
- [5] M. Leurer, Y. Nir and N. Seiberg, *Mass matrix models: The Sequel*, *Nucl. Phys. B* **420** (1994) 468 [[hep-ph/9310320](#)].
- [6] M. Fedele, A. Mastroddi and M. Valli, *Minimal Froggatt-Nielsen textures*, *JHEP* **03** (2021) 135 [[2009.05587](#)].
- [7] C. Cornella, D. Curtin, E.T. Neil and J.O. Thompson, *Mapping and Probing Froggatt-Nielsen Solutions to the Quark Flavor Puzzle*, [2306.08026](#).
- [8] R.D. Peccei and H.R. Quinn, *CP Conservation in the Presence of Instantons*, *Phys. Rev. Lett.* **38** (1977) 1440.
- [9] F. Wilczek, *Problem of Strong P and T Invariance in the Presence of Instantons*, *Phys. Rev. Lett.* **40** (1978) 279.
- [10] S. Weinberg, *A New Light Boson?*, *Phys. Rev. Lett.* **40** (1978) 223.
- [11] L. Di Luzio, M. Giannotti, E. Nardi and L. Visinelli, *The landscape of QCD axion models*, *Phys. Rept.* **870** (2020) 1 [[2003.01100](#)].
- [12] I.G. Irastorza and J. Redondo, *New experimental approaches in the search for axion-like particles*, *Prog. Part. Nucl. Phys.* **102** (2018) 89 [[1801.08127](#)].
- [13] L. Calibbi, F. Goertz, D. Redigolo, R. Ziegler and J. Zupan, *Minimal axion model from flavor*, *Phys. Rev. D* **95** (2017) 095009 [[1612.08040](#)].
- [14] Y. Ema, K. Hamaguchi, T. Moroi and K. Nakayama, *Flaxion: a minimal extension to solve puzzles in the standard model*, *JHEP* **01** (2017) 096 [[1612.05492](#)].
- [15] J. Martin Camalich, M. Pospelov, P.N.H. Vuong, R. Ziegler and J. Zupan, *Quark Flavor Phenomenology of the QCD Axion*, *Phys. Rev. D* **102** (2020) 015023 [[2002.04623](#)].
- [16] H.M. Georgi, L.J. Hall and M.B. Wise, *Grand Unified Models With an Automatic Peccei-Quinn Symmetry*, *Nucl. Phys. B* **192** (1981) 409.
- [17] M. Dine and N. Seiberg, *String Theory and the Strong CP Problem*, *Nucl. Phys. B* **273** (1986) 109.
- [18] S.M. Barr and D. Seckel, *Planck scale corrections to axion models*, *Phys. Rev. D* **46** (1992) 539.

- [19] M. Kamionkowski and J. March-Russell, *Planck scale physics and the Peccei-Quinn mechanism*, *Phys. Lett. B* **282** (1992) 137 [[hep-th/9202003](#)].
- [20] R. Holman, S.D.H. Hsu, T.W. Kephart, E.W. Kolb, R. Watkins and L.M. Widrow, *Solutions to the strong CP problem in a world with gravity*, *Phys. Lett. B* **282** (1992) 132 [[hep-ph/9203206](#)].
- [21] A. Greljo and A.E. Thomsen, *Rising through the ranks: flavor hierarchies from a gauged $SU(2)$ symmetry*, *Eur. Phys. J. C* **84** (2024) 213 [[2309.11547](#)].
- [22] A. Greljo, A.E. Thomsen and H. Tiplom, *Flavor Hierarchies From $SU(2)$ Flavor and Quark-Lepton Unification*, [2406.02687](#).
- [23] J. Davighi and G. Isidori, *Non-universal gauge interactions addressing the inescapable link between Higgs and flavour*, *JHEP* **07** (2023) 147 [[2303.01520](#)].
- [24] A. Greljo and G. Isidori, *Neutrino Anarchy from Flavor Deconstruction*, [2406.01696](#).
- [25] S. Antusch, A. Greljo, B.A. Stefanek and A.E. Thomsen, *$U(2)$ Is Right for Leptons and Left for Quarks*, *Phys. Rev. Lett.* **132** (2024) 151802 [[2311.09288](#)].
- [26] T. Higaki and J. Kawamura, *A low-scale flavon model with a Z_N symmetry*, *JHEP* **03** (2020) 129 [[1911.09127](#)].
- [27] E. Palti, *The Swampland: Introduction and Review*, *Fortsch. Phys.* **67** (2019) 1900037 [[1903.06239](#)].
- [28] L.M. Krauss and F. Wilczek, *Discrete Gauge Symmetry in Continuum Theories*, *Phys. Rev. Lett.* **62** (1989) 1221.
- [29] T. Banks, *Effective Lagrangian Description of Discrete Gauge Symmetries*, *Nucl. Phys. B* **323** (1989) 90.
- [30] J. Preskill and L.M. Krauss, *Local Discrete Symmetry and Quantum Mechanical Hair*, *Nucl. Phys. B* **341** (1990) 50.
- [31] L.E. Ibanez and G.G. Ross, *Discrete gauge symmetry anomalies*, *Phys. Lett. B* **260** (1991) 291.
- [32] B. Gavela, P. Quílez and M. Ramos, *The QCD axion sum rule*, *JHEP* **04** (2024) 056 [[2305.15465](#)].
- [33] F. Björkeröth, E.J. Chun and S.F. King, *Flavourful Axion Phenomenology*, *JHEP* **08** (2018) 117 [[1806.00660](#)].
- [34] M. Bauer, M. Neubert, S. Renner, M. Schnubel and A. Thamm, *Axionlike Particles, Lepton-Flavor Violation, and a New Explanation of a_μ and a_e* , *Phys. Rev. Lett.* **124** (2020) 211803 [[1908.00008](#)].
- [35] M. Bauer, M. Neubert, S. Renner, M. Schnubel and A. Thamm, *Flavor probes of axion-like particles*, *JHEP* **09** (2022) 056 [[2110.10698](#)].
- [36] J. Bonilla, A. de Giorgi, B. Gavela, L. Merlo and M. Ramos, *The cost of an ALP solution to the neutral B-anomalies*, *JHEP* **02** (2023) 138 [[2209.11247](#)].
- [37] C. Cornella, A.M. Galda, M. Neubert and D. Wyler, *$K \rightarrow \pi a$ at next-to-leading order in chiral perturbation theory and updated bounds on ALP couplings*, *JHEP* **06** (2024) 029 [[2308.16903](#)].

- [38] A. Biekötter, J. Fuentes-Martín, A.M. Galda and M. Neubert, *A global analysis of axion-like particle interactions using SMEFT fits*, *JHEP* **09** (2023) 120 [[2307.10372](#)].
- [39] L. Calibbi, T. Li, L. Mukherjee and Y. Yang, *Probing ALP Lepton Flavour Violation at μ TRISTAN*, [2406.13234](#).
- [40] L. Di Luzio, A.W.M. Guerrero, X. Ponce Díaz and S. Rigolin, *Axion-Like Particles in Radiative Quarkonia Decays*, [2402.12454](#).
- [41] S. Knapen, K. Langhoff, T. Opferkuch and D. Redigolo, *A Robust Search for Lepton Flavour Violating Axions at Mu3e*, [2311.17915](#).
- [42] FLAVOUR LATTICE AVERAGING GROUP (FLAG) collaboration, *FLAG Review 2021*, *Eur. Phys. J. C* **82** (2022) 869 [[2111.09849](#)].
- [43] N. Gubernari, M. Reboud, D. van Dyk and J. Virto, *Dispersive analysis of $B \rightarrow K^{(*)}$ and $B_s \rightarrow \phi$ form factors*, *JHEP* **12** (2023) 153 [[2305.06301](#)].
- [44] HPQCD collaboration, *$B \rightarrow K$ and $D \rightarrow K$ form factors from fully relativistic lattice QCD*, *Phys. Rev. D* **107** (2023) 014510 [[2207.12468](#)].
- [45] J.A. Bailey et al., *$B \rightarrow Kl^{+l^-}$ Decay Form Factors from Three-Flavor Lattice QCD*, *Phys. Rev. D* **93** (2016) 025026 [[1509.06235](#)].
- [46] HPQCD collaboration, *Rare decay $B \rightarrow K\ell^+\ell^-$ form factors from lattice QCD*, *Phys. Rev. D* **88** (2013) 054509 [[1306.2384](#)].
- [47] R.R. Horgan, Z. Liu, S. Meinel and M. Wingate, *Lattice QCD calculation of form factors describing the rare decays $B \rightarrow K^*\ell^+\ell^-$ and $B_s \rightarrow \phi\ell^+\ell^-$* , *Phys. Rev. D* **89** (2014) 094501 [[1310.3722](#)].
- [48] R.R. Horgan, Z. Liu, S. Meinel and M. Wingate, *Rare B decays using lattice QCD form factors*, *PoS LATTICE2014* (2015) 372 [[1501.00367](#)].
- [49] E949, E787 collaboration, *Measurement of the $K^+ \rightarrow \pi^+\bar{\nu}\nu$ branching ratio*, *Phys. Rev. D* **77** (2008) 052003 [[0709.1000](#)].
- [50] BABAR collaboration, *Search for $B \rightarrow K^{(*)}\nu\bar{\nu}$ and invisible quarkonium decays*, *Phys. Rev. D* **87** (2013) 112005 [[1303.7465](#)].
- [51] BELLE-II collaboration, *Evidence for $B^+ \rightarrow K^+\nu\bar{\nu}$ Decays*, [2311.14647](#).
- [52] W. Altmannshofer, A. Crivellin, H. Haigh, G. Inguglia and J. Martin Camalich, *Light new physics in $B \rightarrow K^{(*)}\nu\nu^{-}$* , *Phys. Rev. D* **109** (2024) 075008 [[2311.14629](#)].
- [53] P.D. Bolton, S. Fajfer, J.F. Kamenik and M. Novoa-Brunet, *Signatures of Light New Particles in $B \rightarrow K^{(*)}E_{\text{miss}}$* , [2403.13887](#).
- [54] C. Cornella, P. Paradisi and O. Sumensari, *Hunting for ALPs with Lepton Flavor Violation*, *JHEP* **01** (2020) 158 [[1911.06279](#)].
- [55] I. Plakias and O. Sumensari, *Lepton Flavor Violation in Semileptonic Observables*, [2312.14070](#).
- [56] PARTICLE DATA GROUP collaboration, *Review of Particle Physics*, *PTEP* **2022** (2022) 083C01.
- [57] D.M. Straub, *flavio: a Python package for flavour and precision phenomenology in the Standard Model and beyond*, [1810.08132](#).

- [58] BELLE collaboration, *Search for the Lepton Flavor Violating Decays $B^+ \rightarrow K^+ \tau^\pm \ell^\mp$ ($\ell = e, \mu$) at Belle*, *Phys. Rev. Lett.* **130** (2023) 261802 [[2212.04128](#)].
- [59] BABAR collaboration, *A search for the decay modes $B^{+-} \rightarrow h^{+-} \tau^{+-} l$* , *Phys. Rev. D* **86** (2012) 012004 [[1204.2852](#)].
- [60] LHCb collaboration, *Search for the lepton-flavour violating decays $B^0 \rightarrow K^{*0} \tau^\pm \mu^\mp$* , *JHEP* **06** (2023) 143 [[2209.09846](#)].
- [61] A. Greljo, J. Salko, A. Smolkovič and P. Stangl, *Rare b decays meet high-mass Drell-Yan*, *JHEP* **05** (2023) 087 [[2212.10497](#)].
- [62] M. Algueró, A. Biswas, B. Capdevila, S. Descotes-Genon, J. Matias and M. Novoa-Brunet, *To $(b)e$ or not to $(b)e$: no electrons at LHCb*, *Eur. Phys. J. C* **83** (2023) 648 [[2304.07330](#)].
- [63] M. Ciuchini, M. Fedele, E. Franco, A. Paul, L. Silvestrini and M. Valli, *Constraints on lepton universality violation from rare B decays*, *Phys. Rev. D* **107** (2023) 055036 [[2212.10516](#)].
- [64] T. Hurth, F. Mahmoudi and S. Neshatpour, *B anomalies in the post $R_{K^{(*)}}$ era*, *Phys. Rev. D* **108** (2023) 115037 [[2310.05585](#)].
- [65] D. Guadagnoli, C. Normand, S. Simula and L. Vittorio, *Insights on the current semi-leptonic B -decay discrepancies — and how $B_s \rightarrow \mu^+ \mu^- \gamma$ can help*, *JHEP* **10** (2023) 102 [[2308.00034](#)].
- [66] LHCb collaboration, *Test of lepton universality in $b \rightarrow s \ell^+ \ell^-$ decays*, *Phys. Rev. Lett.* **131** (2023) 051803 [[2212.09152](#)].
- [67] LHCb collaboration, *Measurement of lepton universality parameters in $B^+ \rightarrow K^+ \ell^+ \ell^-$ and $B^0 \rightarrow K^{*0} \ell^+ \ell^-$ decays*, *Phys. Rev. D* **108** (2023) 032002 [[2212.09153](#)].
- [68] LHCb collaboration, *Search for hidden-sector bosons in $B^0 \rightarrow K^{*0} \mu^+ \mu^-$ decays*, *Phys. Rev. Lett.* **115** (2015) 161802 [[1508.04094](#)].
- [69] LHCb collaboration, *Search for long-lived scalar particles in $B^+ \rightarrow K^+ \chi(\mu^+ \mu^-)$ decays*, *Phys. Rev. D* **95** (2017) 071101 [[1612.07818](#)].
- [70] M.B. Gavela, R. Houtz, P. Quilez, R. Del Rey and O. Sumensari, *Flavor constraints on electroweak ALP couplings*, *Eur. Phys. J. C* **79** (2019) 369 [[1901.02031](#)].
- [71] M. Bauer, M. Neubert and A. Thamm, *Collider Probes of Axion-Like Particles*, *JHEP* **12** (2017) 044 [[1708.00443](#)].
- [72] NA62 collaboration, *Measurement of the $K \rightarrow \gamma \gamma$ decay*, *Phys. Lett. B* **850** (2024) 138513 [[2311.01837](#)].
- [73] BABAR collaboration, *Search for an Axionlike Particle in B Meson Decays*, *Phys. Rev. Lett.* **128** (2022) 131802 [[2111.01800](#)].
- [74] E.E. Jenkins, A.V. Manohar and P. Stoffer, *Low-Energy Effective Field Theory below the Electroweak Scale: Operators and Matching*, *JHEP* **03** (2018) 016 [[1709.04486](#)].
- [75] J. Fuentes-Martín, M. König, J. Pagès, A.E. Thomsen and F. Wilsch, *A proof of concept for matchete: an automated tool for matching effective theories*, *Eur. Phys. J. C* **83** (2023) 662 [[2212.04510](#)].
- [76] A.J. Buras, D. Guadagnoli and G. Isidori, *On ϵ_K Beyond Lowest Order in the Operator Product Expansion*, *Phys. Lett. B* **688** (2010) 309 [[1002.3612](#)].

- [77] T. Blum et al., *The $K \rightarrow (\pi\pi)_{I=2}$ Decay Amplitude from Lattice QCD*, *Phys. Rev. Lett.* **108** (2012) 141601 [[1111.1699](#)].
- [78] J. Brod and M. Gorbahn, *Next-to-Next-to-Leading-Order Charm-Quark Contribution to the CP Violation Parameter ϵ_K and ΔM_K* , *Phys. Rev. Lett.* **108** (2012) 121801 [[1108.2036](#)].
- [79] RBC/UKQCD collaboration, *Neutral Kaon Mixing Beyond the Standard Model with $n_f = 2 + 1$ Chiral Fermions Part 1: Bare Matrix Elements and Physical Results*, *JHEP* **11** (2016) 001 [[1609.03334](#)].
- [80] D. King, A. Lenz and T. Rauh, *B_s mixing observables and $-V_{td}/V_{ts}$ — from sum rules*, *JHEP* **05** (2019) 034 [[1904.00940](#)].
- [81] R.J. Dowdall, C.T.H. Davies, R.R. Horgan, G.P. Lepage, C.J. Monahan, J. Shigemitsu et al., *Neutral B-meson mixing from full lattice QCD at the physical point*, *Phys. Rev. D* **100** (2019) 094508 [[1907.01025](#)].
- [82] HFLAV collaboration, *Averages of b-hadron, c-hadron, and τ -lepton properties as of 2021*, *Phys. Rev. D* **107** (2023) 052008 [[2206.07501](#)].
- [83] ETM collaboration, *$\Delta S=2$ and $\Delta C=2$ bag parameters in the standard model and beyond from $N_f=2+1+1$ twisted-mass lattice QCD*, *Phys. Rev. D* **92** (2015) 034516 [[1505.06639](#)].
- [84] B. Grzadkowski, M. Iskrzynski, M. Misiak and J. Rosiek, *Dimension-Six Terms in the Standard Model Lagrangian*, *JHEP* **10** (2010) 085 [[1008.4884](#)].
- [85] C. Bobeth, A.J. Buras, A. Celis and M. Jung, *Patterns of Flavour Violation in Models with Vector-Like Quarks*, *JHEP* **04** (2017) 079 [[1609.04783](#)].
- [86] RBC, UKQCD collaboration, *Direct CP violation and the $\Delta I = 1/2$ rule in $K \rightarrow \pi\pi$ decay from the standard model*, *Phys. Rev. D* **102** (2020) 054509 [[2004.09440](#)].
- [87] A.J. Buras and J.-M. Gérard, *Isospin-breaking in ϵ'/ϵ : impact of η_0 at the dawn of the 2020s*, *Eur. Phys. J. C* **80** (2020) 701 [[2005.08976](#)].
- [88] J. Aebischer, C. Bobeth and A.J. Buras, *ϵ'/ϵ in the Standard Model at the Dawn of the 2020s*, *Eur. Phys. J. C* **80** (2020) 705 [[2005.05978](#)].
- [89] J. Aebischer, C. Bobeth, A.J. Buras and J. Kumar, *BSM master formula for ϵ'/ϵ in the WET basis at NLO in QCD*, *JHEP* **12** (2021) 043 [[2107.12391](#)].
- [90] V. Cirigliano, H. Gisbert, A. Pich and A. Rodríguez-Sánchez, *Isospin-violating contributions to ϵ'/ϵ* , *JHEP* **02** (2020) 032 [[1911.01359](#)].
- [91] J. Aebischer, C. Bobeth, A.J. Buras, J.-M. Gérard and D.M. Straub, *Master formula for ϵ'/ϵ beyond the Standard Model*, *Phys. Lett. B* **792** (2019) 465 [[1807.02520](#)].
- [92] L. Lavoura, *General formulae for $f(1) \rightarrow f(2)$ gamma*, *Eur. Phys. J. C* **29** (2003) 191 [[hep-ph/0302221](#)].
- [93] MEG collaboration, *New constraint on the existence of the $\mu^+ \rightarrow e^+\gamma$ decay*, *Phys. Rev. Lett.* **110** (2013) 201801 [[1303.0754](#)].
- [94] MEG collaboration, *Search for the lepton flavour violating decay $\mu^+ \rightarrow e^+\gamma$ with the full dataset of the MEG experiment*, *Eur. Phys. J. C* **76** (2016) 434 [[1605.05081](#)].
- [95] BABAR collaboration, *Searches for Lepton Flavor Violation in the Decays $\tau^\pm \rightarrow e^\pm\gamma$ and $\tau^\pm \rightarrow \mu^\pm\gamma$* , *Phys. Rev. Lett.* **104** (2010) 021802 [[0908.2381](#)].

- [96] BELLE collaboration, *New Search for $\tau \rightarrow \mu\gamma$ and $\tau \rightarrow e\gamma$ Decays at Belle*, *Phys. Lett. B* **666** (2008) 16 [0705.0650].
- [97] A. Crivellin, S. Davidson, G.M. Pruna and A. Signer, *Renormalisation-group improved analysis of $\mu \rightarrow e$ processes in a systematic effective-field-theory approach*, *JHEP* **05** (2017) 117 [1702.03020].
- [98] R. Kitano, M. Koike and Y. Okada, *Detailed calculation of lepton flavor violating muon electron conversion rate for various nuclei*, *Phys. Rev. D* **66** (2002) 096002 [hep-ph/0203110].
- [99] V. Cirigliano, R. Kitano, Y. Okada and P. Tuzon, *On the model discriminating power of $\mu \rightarrow e$ conversion in nuclei*, *Phys. Rev. D* **80** (2009) 013002 [0904.0957].
- [100] M.A. Shifman, A.I. Vainshtein and V.I. Zakharov, *Remarks on Higgs Boson Interactions with Nucleons*, *Phys. Lett. B* **78** (1978) 443.
- [101] A. Crivellin, M. Hoferichter and M. Procura, *Improved predictions for $\mu \rightarrow e$ conversion in nuclei and Higgs-induced lepton flavor violation*, *Phys. Rev. D* **89** (2014) 093024 [1404.7134].
- [102] M. Hoferichter, J. Ruiz de Elvira, B. Kubis and U.-G. Meißner, *High-Precision Determination of the Pion-Nucleon σ Term from Roy-Steiner Equations*, *Phys. Rev. Lett.* **115** (2015) 092301 [1506.04142].
- [103] A. Crivellin, M. Hoferichter and M. Procura, *Accurate evaluation of hadronic uncertainties in spin-independent WIMP-nucleon scattering: Disentangling two- and three-flavor effects*, *Phys. Rev. D* **89** (2014) 054021 [1312.4951].
- [104] P. Junnarkar and A. Walker-Loud, *Scalar strange content of the nucleon from lattice QCD*, *Phys. Rev. D* **87** (2013) 114510 [1301.1114].
- [105] SINDRUM II collaboration, *A Search for muon to electron conversion in muonic gold*, *Eur. Phys. J. C* **47** (2006) 337.
- [106] T. Suzuki, D.F. Measday and J.P. Roalsvig, *Total Nuclear Capture Rates for Negative Muons*, *Phys. Rev. C* **35** (1987) 2212.
- [107] A. Crivellin, F. Kirk, C.A. Manzari and M. Montull, *Global Electroweak Fit and Vector-Like Leptons in Light of the Cabibbo Angle Anomaly*, *JHEP* **12** (2020) 166 [2008.01113].
- [108] A. Jodidio et al., *Search for Right-Handed Currents in Muon Decay*, *Phys. Rev. D* **34** (1986) 1967.
- [109] TWIST collaboration, *Search for two body muon decay signals*, *Phys. Rev. D* **91** (2015) 052020 [1409.0638].
- [110] BELLE-II collaboration, *Search for Lepton-Flavor-Violating τ Decays to a Lepton and an Invisible Boson at Belle II*, *Phys. Rev. Lett.* **130** (2023) 181803 [2212.03634].
- [111] BELLE-II collaboration, *Search for lepton-flavor-violating $\tau^- \rightarrow \mu^- \mu^+ \mu^-$ decays at Belle II*, [2405.07386](#).
- [112] SINDRUM collaboration, *Search for the Decay $\mu^+ \rightarrow e^+ e^+ e^-$* , *Nucl. Phys. B* **299** (1988) 1.
- [113] J. Heeck and W. Rodejohann, *Lepton flavor violation with displaced vertices*, *Phys. Lett. B* **776** (2018) 385 [1710.02062].
- [114] K. Cheung, A. Soffer, Z.S. Wang and Y.-H. Wu, *Probing charged lepton flavor violation with axion-like particles at Belle II*, *JHEP* **11** (2021) 218 [2108.11094].

- [115] SINDRUM collaboration, *Limits for Shortlived Neutral Particles Emitted μ^+ or π^+ Decay*, *Phys. Lett. B* **175** (1986) 101.
- [116] R.D. Bolton et al., *Search for Rare Muon Decays with the Crystal Box Detector*, *Phys. Rev. D* **38** (1988) 2077.
- [117] H. Natori, *Search for a Lepton Flavor Violating Muon Decay Mediated by a New Light Neutral Particle with the MEG Detector*, Ph.D. thesis, Tokyo U., 2012.
- [118] MEG collaboration, *Search for lepton flavour violating muon decay mediated by a new light particle in the MEG experiment*, *Eur. Phys. J. C* **80** (2020) 858 [2005.00339].
- [119] J. Aebischer, J. Kumar, P. Stangl and D.M. Straub, *A Global Likelihood for Precision Constraints and Flavour Anomalies*, *Eur. Phys. J. C* **79** (2019) 509 [1810.07698].
- [120] T.S. Roussy et al., *An improved bound on the electron’s electric dipole moment*, *Science* **381** (2023) adg4084 [2212.11841].
- [121] C. Abel et al., *Measurement of the Permanent Electric Dipole Moment of the Neutron*, *Phys. Rev. Lett.* **124** (2020) 081803 [2001.11966].
- [122] J. Kley, T. Theil, E. Venturini and A. Weiler, *Electric dipole moments at one-loop in the dimension-6 SMEFT*, *Eur. Phys. J. C* **82** (2022) 926 [2109.15085].
- [123] L. Di Luzio, R. Gröber and P. Paradisi, *Hunting for CP-violating axionlike particle interactions*, *Phys. Rev. D* **104** (2021) 095027 [2010.13760].
- [124] C. O’Hare, “cajohare/axionlimits: Axionlimits.” <https://cajohare.github.io/AxionLimits/>, July, 2020. 10.5281/zenodo.3932430.
- [125] P.F. de Salas, M. Lattanzi, G. Mangano, G. Miele, S. Pastor and O. Pisanti, *Bounds on very low reheating scenarios after Planck*, *Phys. Rev. D* **92** (2015) 123534 [1511.00672].
- [126] K. Mimasu and V. Sanz, *ALPs at Colliders*, *JHEP* **06** (2015) 173 [1409.4792].
- [127] I. Brivio, M.B. Gavela, L. Merlo, K. Mimasu, J.M. No, R. del Rey et al., *ALPs Effective Field Theory and Collider Signatures*, *Eur. Phys. J. C* **77** (2017) 572 [1701.05379].
- [128] A. Carmona, F. Elahi, C. Scherb and P. Schwaller, *The ALPs from the top: searching for long lived axion-like particles from exotic top decays*, *JHEP* **07** (2022) 122 [2202.09371].
- [129] F. Esser, M. Madigan, V. Sanz and M. Ubiali, *On the coupling of axion-like particles to the top quark*, *JHEP* **09** (2023) 063 [2303.17634].
- [130] S. Blasi, F. Maltoni, A. Mariotti, K. Mimasu, D. Pagani and S. Tentori, *Top-philic ALP phenomenology at the LHC: the elusive mass-window*, *JHEP* **06** (2024) 077 [2311.16048].
- [131] L. Rygaard, J. Niedziela, R. Schäfer, S. Bruggisser, J. Alimena, S. Westhoff et al., *Top Secrets: long-lived ALPs in top production*, *JHEP* **10** (2023) 138 [2306.08686].
- [132] A.V. Phan and S. Westhoff, *Precise tests of the axion coupling to tops*, *JHEP* **05** (2024) 075 [2312.00872].
- [133] T. Li, Z. Qian, M.A. Schmidt and M. Yuan, *The quark flavor-violating ALPs in light of B mesons and hadron colliders*, *JHEP* **05** (2024) 232 [2402.14232].
- [134] M. Bauer, T. Schell and T. Plehn, *Hunting the Flavon*, *Phys. Rev. D* **94** (2016) 056003 [1603.06950].

- [135] ATLAS collaboration, *Search for pair-production of vector-like quarks in lepton+jets final states containing at least one b-tagged jet using the Run 2 data from the ATLAS experiment*, *Phys. Lett. B* **854** (2024) 138743 [[2401.17165](#)].
- [136] CMS collaboration, *Review of searches for vector-like quarks, vector-like leptons, and heavy neutral leptons in proton-proton collisions at $\sqrt{s} = 13$ TeV at the CMS experiment*, [2405.17605](#).
- [137] L. Calibbi, D. Redigolo, R. Ziegler and J. Zupan, *Looking forward to lepton-flavor-violating ALPs*, *JHEP* **09** (2021) 173 [[2006.04795](#)].
- [138] MU2E collaboration, *The Mu2e Experiment*, *Front. in Phys.* **7** (2019) 1 [[1901.11099](#)].
- [139] COMET collaboration, *Search for Muon-to-Electron Conversion with the COMET Experiment \dagger* , *Universe* **8** (2022) 196 [[2203.06365](#)].
- [140] A. Carmona, C. Scherb and P. Schwaller, *Charming ALPs*, *JHEP* **08** (2021) 121 [[2101.07803](#)].
- [141] G.-y. Huang and S. Zhou, *Precise Values of Running Quark and Lepton Masses in the Standard Model*, *Phys. Rev. D* **103** (2021) 016010 [[2009.04851](#)].